

## PAPER

Cite this: *Catal. Sci. Technol.*, 2016,  
6, 8036

# Co-decorated Cu alloy catalyst for C<sub>2</sub> oxygenate and ethanol formation from syngas on Cu-based catalyst: insight into the role of Co and Cu as well as the improved selectivity†

Riguang Zhang, Fu Liu and Baojun Wang\*

Co-decorated Cu alloy, a potential material for use in syngas conversion based on less expensive Cu metal, can efficiently promote the formation of C<sub>2</sub> oxygenates and ethanol. Herein, the mechanisms of C<sub>2</sub> oxygenate and ethanol formation from syngas on Co-decorated Cu alloy catalyst have been investigated to probe into the role of Co and Cu and identify the catalytic selectivity of Cu catalysts toward C<sub>2</sub> oxygenates and ethanol. DFT calculations with microkinetic modeling have been performed, and the Co-decorated Cu alloy catalyst is modeled using Co-doped Cu(211) surface. Our results suggest that CO initial adsorption and activation occur at the Cu sites of Co-doped Cu(211). CO prefers to be hydrogenated to CHO at the Cu site, and subsequently, CHO species at the Cu site easily migrate to the most stable Co–Cu mixed site. Starting from CHO species adsorbed at the Co–Cu mixed site, CH<sub>2</sub> and CH<sub>3</sub> species are the most favorable CH<sub>x</sub> monomers formed *via* H-assisted CH<sub>x</sub>O (*x* = 2, 3) dissociation, which are more favorable than CH<sub>3</sub>OH formation both thermodynamically and dynamically, suggesting that the CoCu(211) surface can provide more CH<sub>x</sub> resources for C–C chain formation. Further, starting from CH<sub>2</sub> and CH<sub>3</sub> species, ethanol is formed by CO insertion into CH<sub>2</sub> and CH<sub>3</sub> to CH<sub>2</sub>CO and CH<sub>3</sub>CO, respectively; subsequently, CH<sub>2</sub>CO and CH<sub>3</sub>CO are successively hydrogenated to ethanol *via* CH<sub>2</sub>CHO, CH<sub>3</sub>CHO and CH<sub>3</sub>CH<sub>2</sub>O intermediates. Based on microkinetic modeling, the CoCu(211) surface is highly selective for ethanol rather than methanol and methane. Moreover, the function of Cu is to provide the undissociated CO/CHO at the Cu sites; Co promotes CH<sub>x</sub> formation by accelerating the C–O bond cleavage of CH<sub>x</sub>O species, and the synergetic effect of Co and Cu facilitates C–C chain formation, which is typical of a “dual-site” mechanism. Thus, the synergetic effects between the active Co and Cu sites promote the formation of C<sub>2</sub> oxygenates and ethanol; the productivity and selectivity of ethanol over the Co-decorated Cu-based catalyst can be improved compared to that of the pure Cu catalyst. In addition, we believe that the insight derived from this study can be valuable for the design of other types of Cu-based catalysts involved in C<sub>2</sub> oxygenate synthesis from syngas.

Received 7th June 2016,  
Accepted 20th September 2016

DOI: 10.1039/c6cy01239f

[www.rsc.org/catalysis](http://www.rsc.org/catalysis)

## 1. Introduction

Syngas (CO and H<sub>2</sub>) conversion to C<sub>2</sub> oxygenates<sup>1,2</sup> has attracted much attention due to the increasing demand for energy and the limited availability of easily accessible petro-

leum resources.<sup>3</sup> Four types of catalysts exist for C<sub>2</sub> oxygenate formation from syngas:<sup>4–8</sup> Rh-based and Mo-based catalysts, modified Fischer–Tropsch (F–T) synthesis catalysts and Cu-based catalysts. Rh-based catalysts exhibit high selectivity to C<sub>2</sub> oxygenates, but Rh cannot be commercially used due to its high cost. Mo-based catalysts have a high catalytic performance as well as an excellent sulfur tolerance; however, the reaction must be carried out at high pressures and temperatures and usually has a long activity induction period during the reaction, which limit the application of this process. Modified F–T synthesis catalysts (Fe- or Co-based) have been reported to generate a great deal of hydrocarbons, which decrease the yield of alcohol. Much less expensive Cu-based catalysts are preferentially selected for methanol formation rather than C<sub>2</sub> oxygenates. Therefore, in order to obtain both

Key Laboratory of Coal Science and Technology of Ministry of Education and Shanxi Province, Taiyuan University of Technology, Taiyuan 030024, Shanxi, PR China. E-mail: wangbaojun@tyut.edu.cn, wbj@tyut.edu.cn;  
Fax: +86 351 6041237; Tel: +86 351 6018239

† Electronic supplementary information (ESI) available: Detailed descriptions about the elementary reactions involved in the formation of CH<sub>x</sub> (*x* = 1–3), C<sub>2</sub> hydrocarbons and oxygenates, and the microkinetic modeling over the CoCu(211) surface as well as the differential charge density have been presented. See DOI: 10.1039/c6cy01239f

lower cost and higher catalytic performance of catalysts, extensive studies have been carried out to design a variety of bimetallic materials, such as bimetallic Co–Cu,<sup>9–14</sup> Fe–Cu,<sup>15–18</sup> and Rh–Cu<sup>19,20</sup> catalysts. Among them, Co–Cu bimetallic catalysts are thought to be the most promising catalysts owing to their high selectivity to higher alcohol and inexpensive cost.

Co–Cu bimetallic catalysts are of two types; one type is Cu-decorated Co-based catalysts and the other is Co-decorated Cu-based catalysts. Recently, in the case of Cu-decorated Co-based catalysts, extensive studies have been carried out. For example, Xiang *et al.*<sup>21</sup> have experimentally designed a highly selective Co–Cu nanoscale catalyst consisting of a Co-rich core structure and a Cu-dominated mixed shell, and the selectivity to long chain alcohols is superior to that of traditional Co–Cu catalysts. Moreover, Prieto *et al.*<sup>22</sup> have identified a Co–Cu alloy phase with Co-rich compositions as the ideal catalyst surface for long-chain alcohols by theoretical and experimental studies. The interactions of the different components in Co/CuZnO catalysts involved in CO hydrogenation have been investigated by Mo *et al.*<sup>23</sup> using steady state isotopic transient kinetic analysis (SSITKA), suggesting that the addition of Cu into Co significantly promotes the formation of more C<sub>2+</sub> oxygenates by blocking a significant fraction of Co sites for hydrocarbon synthesis. A similar conclusion has been confirmed by Xu *et al.*<sup>24</sup> on both pure and Cu-doped Co(0001) surfaces for C<sub>2</sub> oxygenate from syngas using density functional theory (DFT) calculations, and the nature of the Cu promotion was mainly attributed to the geometric effect rather than an electronic effect; the geometric effect provides the undissociated CO/CHO.

Based on less expensive Cu materials for Co-decorated Cu-based catalysts, a large number of experimental studies have proved that Co–Cu bimetallic catalysts with Cu-rich compositions also show high selectivity toward higher alcohols. Subramanian *et al.*<sup>25</sup> have synthesized two sets of Co–Cu nanoparticles with novel structures by using wet chemical methods, Co core–Cu shell (Co@Cu) and Co–Cu mixed nanoparticles, in which the Co–Cu mixed nanoparticles with Cu-rich compositions (Co : Cu = 1 : 24) exhibit a greater selectivity toward ethanol and C<sub>2+</sub> oxygenates. Anton *et al.*<sup>26</sup> have investigated the relationships between structure and activity for Co-modified Cu-based catalysts by co-precipitation using Cu, Co, Zn and Al nitrates in higher alcohol synthesis, indicating that an improved intimate interface contact between the large metallic Cu<sup>0</sup> nanoparticles detected by XRD and the X-ray amorphous metallic Co surface species probed by XPS favors the synthesis of higher alcohols. Pei *et al.*<sup>27</sup> have investigated the formation of higher alcohols on activated carbon supported CoCuMn catalysts, in which large Cu particles were decorated by small spherical Co nanoparticles; such a structure is responsible for the favored formation of higher alcohols. Gao *et al.*<sup>28</sup> have designed the CuCo-alloy catalysts with a Cu-rich core and a CuCo-alloy shell, which is stable and recyclable owing to the unique electronic and geometric interaction between Cu and Co and exhibits good selectivity toward higher alcohols.

On the other hand, it is widely accepted that the formation mechanism of C<sub>2</sub> oxygenates and hydrocarbons from syngas involves two key steps:<sup>19,29–31</sup> one is the surface hydrocarbon species (CH<sub>x</sub>), produced by direct CO dissociation into C, followed by hydrogenation (carbide mechanism), or *vice versa* (hydrogen-assisted CO dissociation mechanism); the other is C–C chain formation, CO/CHO insertion into the CH<sub>x</sub> monomer and carbene coupling leading to the formation of C<sub>2</sub> oxygenates and hydrocarbons, respectively.

So far, for Co–Cu bimetallic catalysts, although previous experimental studies have suggested that the synergistic effect<sup>22,27,32–36</sup> between Cu and Co for higher alcohols may be critical, to the best of our knowledge, the underlying formation mechanism of C<sub>2</sub> oxygenates from syngas as well as the roles of Co and Cu over Co-decorated Cu-based catalysts, namely, Co–Cu bimetallic catalysts with Cu-rich compositions, still remains unclear at the molecular level.

In this study, DFT calculations together with microkinetic modeling have been performed to probe into the underlying mechanism of syngas conversion to C<sub>2</sub> oxygenates and hydrocarbons over Co–Cu bimetallic catalysts with Cu-rich compositions; the roles of Co and Cu for Co–Cu bimetallic catalysts in syngas conversion to C<sub>2</sub> oxygenates and hydrocarbons will be clarified at a molecular level. Meanwhile, a clear picture of C<sub>2</sub> oxygenate and hydrocarbon formation from syngas over Co–Cu bimetallic catalysts with Cu-rich compositions can be obtained, and the results are expected to readdress the following puzzles: What are the roles of Co and Cu? How does the Co-promoter promote high alcohol productivity and selectivity? Further, the results will not only help us better understand the underlying mechanism of C<sub>2</sub> oxygenates and hydrocarbons and the roles of Cu and Co over Co–Cu bimetallic catalysts with Cu-rich compositions at a molecular level but also provide a reference for studies about other types of metal M-decorated Cu-based catalyst materials, which can serve as a basis for the selective modification of Cu-based catalyst materials to improve the catalytic performance toward the desired products from syngas.

## 2. Computational details

### 2.1 Surface model

For the Co–Cu bimetallic catalyst, two types of models may exist: alloys and inter-metallic catalysts. So far, a large number of experimental studies<sup>11–14,21,25,33,37–40</sup> have confirmed that Co–Cu alloy exhibits high selectivity toward higher alcohols over Co–Cu bimetallic catalysts although the low solubility between Co and Cu exists.<sup>41</sup> Thus, the alloy model has been chosen; meanwhile, Cu prefers to segregate over the surface<sup>42</sup> because of the smaller surface energy compared to Co (1.934 J m<sup>-2</sup> vs. 2.709 J m<sup>-2</sup>).<sup>43</sup> Moreover, the interaction of Co with Cu, especially the near-surface region with a Cu-rich surface configuration, has been observed under exposure to syngas atmospheres,<sup>21,44</sup> which plays a significant role in the formation of higher alcohols. As a result, the

Co–Cu bimetallic catalyst with a Cu-rich surface has been examined in this study. Of course, the inter-metallic catalyst model is also important to investigate  $C_2$  oxygenate formation from syngas over Co–Cu bimetallic catalyst, which will be carried out in our next work.

It has been evidenced that metal surfaces are not always perfect under a realistic condition, and surface defects are crucial to the properties of metals, especially surface reactivity.<sup>45–49</sup> Moreover, surface defects can enhance the surface catalytic activity,<sup>50–56</sup> and the step site is the most common surface defect for metal catalysts. A stepped (211) surface consists of the (111) terrace and the (100)-type step, which presents a better activity in catalytic reactions.<sup>57–59</sup> For example, Behrens *et al.*<sup>60</sup> have investigated  $CH_3OH$  formation *via* CO and  $CO_2$  hydrogenation on Cu(111) and Cu(211) surfaces, suggesting that the activity is increased at the step site of the Cu(211) surface compared to that at the flat Cu(111) surface. Catapan *et al.*<sup>59</sup> have investigated the water–gas shift reaction on Ni(111) and Ni(211) surfaces, indicating that formate formation is favorable at the step site of the stepped Ni(211) surface owing to its high stability and lower barrier of  $CO_2$  hydrogenation. Kapur *et al.*<sup>61</sup> have found that  $C_2$  oxygenate formation is more favorable on the stepped Rh(211) surface compared to that on the flat Rh(111) surface. In addition, the dissociation of CO (ref. 51) and NO (ref. 62) on the stepped Rh(211) surface has a lower activation barrier compared to those on the flat Rh(111) surface. Therefore, in this study, the stepped Cu(211) surface is employed to model the Cu catalyst.

In this work, a  $p(2 \times 3)$  Co-doped Cu(211) surface with an eight-layer slab is used to model the Co-decorated Cu-based bimetallic catalyst with a Cu-rich surface configuration; a 10 Å vacuum spacing between slabs is set to ensure that no significant interaction between the slabs occurs. The upper five layers together with the adsorbed species are allowed to relax, and the bottom three layers are kept at their bulk position.

For the stepped Co-doped Cu(211) surface, a single Co atom can be doped at three possible sites of the Cu(211) surface: a step edge, a terrace, or a step base site (see Fig. 1(a)). As a result, the most favorable configuration of the Co-doped Cu(211) surface can be obtained according to the substitution energy,  $E_{\text{sub}}$ ,<sup>63,64</sup>

$$E_{\text{sub}} = E_{\text{Co}} + E_{\text{Cu}(211)} - E_{\text{Cu}} - E_{\text{CoCu}(211)}$$

where  $E_{\text{sub}}$  is the substitution energy of the Co-doped Cu(211) surface, and  $E_{\text{Cu}(211)}$  and  $E_{\text{CoCu}(211)}$  are the total energies of the Cu(211) and Co-doped Cu(211) surfaces, respectively.  $E_{\text{Cu}}$  and  $E_{\text{Co}}$  are the total energies of the single Cu or Co atom, respectively. According to this definition, a smaller  $E_{\text{sub}}$  denotes easier replacement of a Cu atom by a Co atom.

Among the three sites, the model with a Co atom at the step edge is found to be the most easily formed; this model needs only a substitution energy of  $4.1 \text{ kJ mol}^{-1}$ , whereas the other two models require substitution energies of 39.9 and

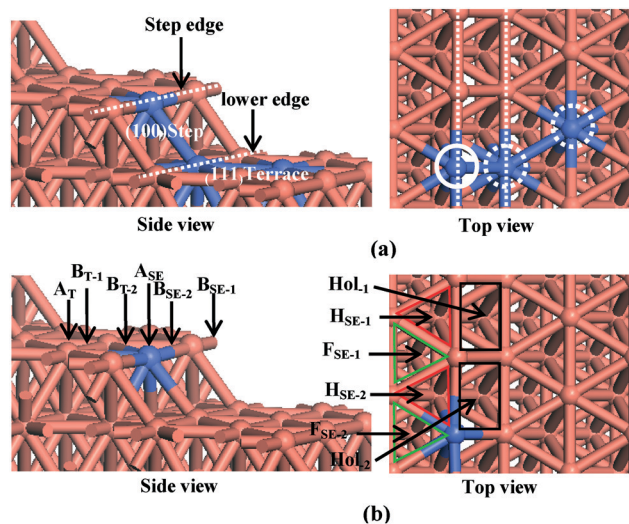


Fig. 1 The surface morphology of (a) Co-doped Cu(211) surface with a Co atom at different sites, (b) Co-doped Cu(211) surface with a Cu atom at the step edge replaced by a Co atom. The blue and orange balls denote Co and Cu atoms, respectively.  $A_{\text{SE}}$ ,  $B_{\text{SE}}$ ,  $F_{\text{SE}}$  and  $H_{\text{SE}}$  refer to the atop, bridge, fcc, and hcp sites at the step edge (SE).  $F_{\text{LE}}$  and  $H_{\text{LE}}$  refer to the fcc and hcp sites at the lower edge (LE).  $A_{\text{T}}$  and  $B_{\text{T}}$  refer to the atop and bridge sites on the (111) terrace, respectively, and  $H_{\text{ol}}$  refers to the hollow adsorption site on the stepped surface.

$37.3 \text{ kJ mol}^{-1}$ . As shown in Fig. 1(b), the system with a Cu atom at the step edge replaced by a Co atom is employed to model the Co-doped Cu(211) surface, which is also named as the CoCu(211) surface in this study. The CoCu(211) surface has nine different adsorption sites: the step edge (atop, bridge, fcc, and hcp), lower edge (fcc and hcp), terrace (atop and bridge), and (100) step (hollow site).

## 2.2 Computational methods

All calculations have been carried out at the level of density functional theory within the Vienna *Ab initio* simulation package (VASP);<sup>65,66</sup> the electron–ion interactions are expressed by the projector-augmented wave (PAW) method.<sup>67,68</sup> The generalized gradient approximation (GGA) proposed by Perdew and Wang (PW91)<sup>69,70</sup> is used to describe the exchange–correlation energies and potential. Due to the magnetic properties of Co, spin-polarized<sup>71</sup> calculations performed for Co systems correctly account for the magnetic properties with a plane wave cutoff energy of 400 eV. The Brillouin zone is sampled by a  $4 \times 4 \times 1$   $k$ -point grid generated *via* the Monkhorst–Pack procedure.<sup>72,73</sup> The geometry optimization will be converged when the energy differences between two electronic optimization steps are lower than  $5 \times 10^{-6} \text{ eV}$  and the forces for ions are smaller than  $0.01 \text{ eV \AA}^{-1}$ .

The adsorption energy with the zero-point correction ( $E_{\text{ads}}$ ) is calculated using eqn (1) and (2):

$$E_{\text{ads}} = (E_{\text{species}} + E_{\text{slab}} - E_{\text{slab/species}}) + \Delta ZPE_{\text{ads}} \quad (1)$$

$$\Delta ZPE_{\text{ads}} = \left( \sum_{i=1}^{\text{Vibrations}} \frac{h\nu_i}{2} \right)_{\text{gas}} - \left( \sum_{i=1}^{\text{Vibrations}} \frac{h\nu_i}{2} \right)_{\text{adsorbed}} \quad (2)$$

where  $E_{\text{slab}}$ ,  $E_{\text{species}}$  and  $E_{\text{species/slab}}$  are the total energies of the slab surface, the free species, and the slab surface together with the adsorbed species in the equilibrium state, respectively.  $\Delta ZPE_{\text{ads}}$  refers to the zero-point vibrational energy (ZPE) correction for the adsorption energy. Eqn (2) is used to calculate the ZPE correction *via* the vibrational frequencies for the species including the gas phase and the adsorbed state. In eqn (2),  $h$  is Planck's constant and  $\nu_i$  refers to frequency. With the definition of adsorption energy, more positive values reflect the strong interactions between the adsorbed species and the slab surface.

To study the minimum energy reaction pathways, the climbing-image nudged elastic band method (CI-NEB)<sup>74,75</sup> is employed to find saddle points between the known reactants and the products, and the transition states are optimized using the dimer method.<sup>76,77</sup> In this study, the optimized transition state structures will be converged when the forces for all atoms are less than 0.05 eV Å<sup>-1</sup>, and the vibrational frequencies are also calculated to confirm the transition state with only one imaginary frequency.

For a reaction such as R (reactant) → P (product) on the CoCu(211) surface, the activation barrier with the zero-point correction ( $E_a$ ) is calculated according to eqn (3) and (4):<sup>78</sup>

$$E_a = (E_{\text{TS}} - E_{\text{R}}) + \Delta ZPE_{\text{barrier}} \quad (3)$$

where  $E_{\text{R}}$  and  $E_{\text{TS}}$  are the total energies of the reactant and the transition state, respectively, and  $\Delta ZPE_{\text{barrier}}$  refers to the ZPE correction for the reaction barrier. The ZPE correction for the activation barrier is determined from the eqn (4):

$$\Delta ZPE_{\text{barrier}} = \left( \sum_{i=1}^{\text{Vibrations}} \frac{h\nu_i}{2} \right)_{\text{TS}} - \left( \sum_{i=1}^{\text{Vibrations}} \frac{h\nu_i}{2} \right)_{\text{R}} \quad (4)$$

The first term includes the vibrational frequencies of the species in the TS, in which the imaginary frequency has not been considered, and the second term includes the vibrational frequencies of the adsorbed reactants.

The reaction energy with the zero-point correction ( $\Delta E$ ) is calculated using eqn (5) and (6):

$$\Delta E = (E_{\text{P}} - E_{\text{R}}) + \Delta ZPE_{\text{energy}} \quad (5)$$

$$\Delta ZPE_{\text{energy}} = \left( \sum_{i=1}^{\text{Vibrations}} \frac{h\nu_i}{2} \right)_{\text{P}} - \left( \sum_{i=1}^{\text{Vibrations}} \frac{h\nu_i}{2} \right)_{\text{R}} \quad (6)$$

$\Delta ZPE_{\text{energy}}$  refers to the ZPE correction for the reaction energy, which is determined by the vibrational frequencies of the reactants and products.

Furthermore, Co–Cu bimetallic catalysts show good catalytic activity toward syngas conversion at the temperature

range of 500–600 K;<sup>14,25</sup> as a result, we have calculated the reaction rate constants involved in the formation of CH<sub>x</sub>, C<sub>2</sub> oxygenates and hydrocarbons from syngas using the harmonic transition state theory<sup>79</sup> at the temperature of 500, 525, 550, 575 and 600 K. The rate constant ( $k$ ) can be obtained using eqn (7):

$$k = \frac{k_{\text{B}}T}{h} \frac{q_{\text{TS}}}{q_{\text{R}}} \exp\left(-\frac{E_a}{k_{\text{B}}T}\right) \quad (7)$$

where  $k_{\text{B}}$  is the Boltzmann constant,  $T$  is the absolute temperature,  $E_a$  is the activation barrier with the zero-point correction. The partition functions ( $q$ ) are calculated using eqn (8), where  $\nu_i$  is the vibrational frequency.

$$q = \frac{1}{\prod_{i=1}^{\text{Vibrations}} \left(1 - \exp\left(-\frac{h\nu_i}{k_{\text{B}}T}\right)\right)} \quad (8)$$

## 3. Results and discussion

### 3.1 Adsorptions of all possible species

In this section, a detailed investigation of the stable adsorption configurations of all possible adsorbed species involved in the formation of C<sub>2</sub> oxygenates and hydrocarbons from syngas has been carried out on the CoCu(211) surface. The most stable adsorption configurations of these species are presented in Fig. 2, and the corresponding adsorption energy and key geometrical parameters are listed in Table 1.

**3.1.1 C, O, CO, H, OH, H<sub>2</sub>O, CH<sub>x</sub> (x = 1–3), C<sub>2</sub>H<sub>4</sub>, CH<sub>4</sub>, C<sub>2</sub>H<sub>6</sub>.** Since both CO and H are the initial reactants, CO and H can be widely adsorbed over the CoCu(211) surface; we have considered all possible adsorption sites around the Co site, Co–Cu mixed site, and Cu site on the CoCu(211) surface, respectively. Our results show that CO prefers to adsorb at the atop-SE Co site *via* a Co–C bond; meanwhile, CO is also adsorbed at the bridge-SE-1 Cu site; the corresponding adsorption energies are 218.8 and 89.5 kJ mol<sup>-1</sup>, respectively. H binds at the fcc-SE-1 Cu site and the bridge-SE-2 Co–Cu mixed site, and the corresponding adsorption energies are 212.2 and 252.9 kJ mol<sup>-1</sup>, respectively.

C and O prefer to adsorb at the hollow-2 and the hcp-SE-2 Co–Cu mixed sites with the corresponding adsorption energies of 677.1 and 577.4 kJ mol<sup>-1</sup>, respectively. OH adsorbs at the bridge-SE-2 Co–Cu mixed site with an adsorption energy of 387.7 kJ mol<sup>-1</sup>. H<sub>2</sub>O adsorbs at the atop-SE Co site *via* O atom with an adsorption energy of 63.7 kJ mol<sup>-1</sup>.

CH adsorbs at the hollow-2 site *via* a C atom with an adsorption energy of 593.5 kJ mol<sup>-1</sup>. Both CH<sub>2</sub> and CH<sub>3</sub> are adsorbed at the bridge-SE-2 Co–Cu mixed sites with the corresponding adsorption energies of 407.4 and 221.3 kJ mol<sup>-1</sup>, respectively. C<sub>2</sub>H<sub>4</sub> molecules prefer to adsorb at the atop-SE Co site *via* C<sub>1</sub> and C<sub>2</sub> atoms with the adsorption energy of 139.9 kJ mol<sup>-1</sup>.

CH<sub>4</sub> and C<sub>2</sub>H<sub>6</sub> are weakly adsorbed upon the surface, which are typical of physisorption, with the adsorption energies of 13.6 and 24.0 kJ mol<sup>-1</sup>, respectively.

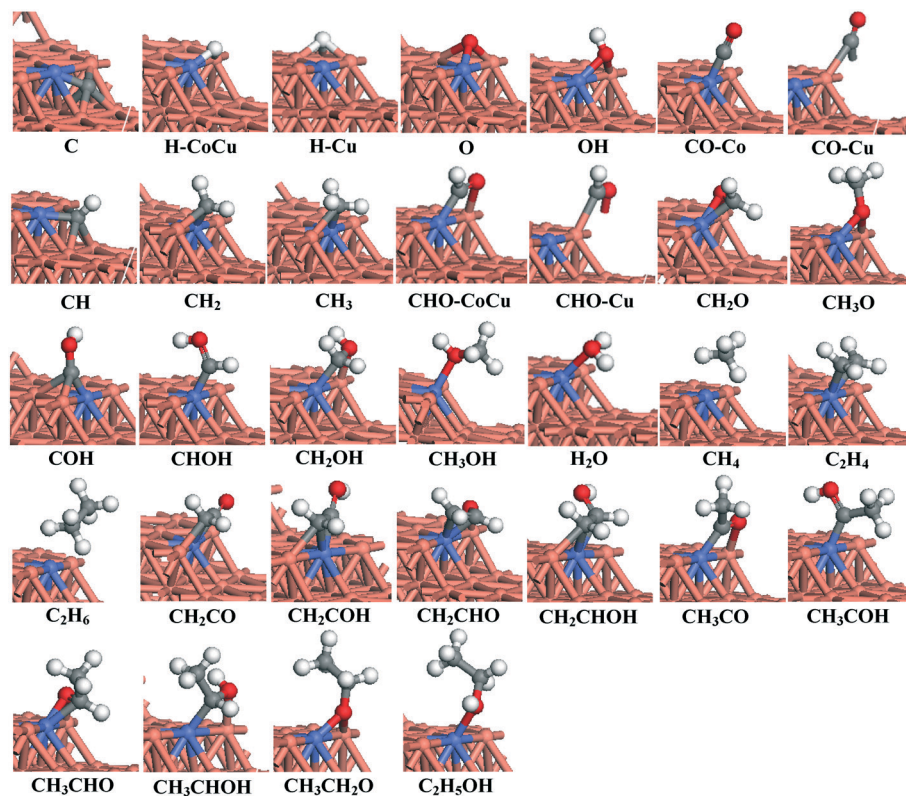


Fig. 2 The most stable adsorption configurations of the surface species involved in  $C_2$  oxygenate and hydrocarbon synthesis from syngas on the CoCu(211) surface. Grey, red, white, orange and blue balls denote C, O, H, Cu and Co atoms, respectively.

**3.1.2  $CH_xO$  ( $x = 1-3$ ),  $CH_xOH$  ( $x = 0-3$ ).** Both CHO and  $CH_2O$  prefer to adsorb at the bridge-SE-2 Co–Cu mixed sites *via* both C and O, which have the corresponding adsorption energies of 264.8 and 148.8  $\text{kJ mol}^{-1}$ , respectively, while  $CH_3O$  is adsorbed at the bridge-SE-2 Co–Cu mixed site *via* an O atom with an adsorption energy of 294.8  $\text{kJ mol}^{-1}$ .

COH adsorbs at the hep-SE-2 Co–Cu mixed site *via* a C atom with the C–O bond perpendicular to the surface, and the adsorption energy is 386.2  $\text{kJ mol}^{-1}$ .  $CH_xOH$  ( $x = 1-3$ ) species have quite different adsorption configurations and energies, CHOH *via* a C atom and  $CH_3OH$  *via* an O atom are adsorbed at the atop-SE Co sites, whereas  $CH_2OH$  is adsorbed at the bridge-SE-2 Co–Cu mixed site *via* both C and O atoms; the adsorption energies of CHOH,  $CH_2OH$ , and  $CH_3OH$  are 323.4, 213.3 and 71.3  $\text{kJ mol}^{-1}$ , respectively.

**3.1.3  $CH_xCO$ ,  $CH_xCOH$ ,  $CH_xCHO$ ,  $CH_xCHOH$  ( $x = 2, 3$ ),  $CH_3CH_2O$ ,  $CH_3CH_2OH$ .**  $CH_2CO$ ,  $CH_2COH$  and  $CH_2CHOH$  prefer to adsorb at the bridge-SE-2 Co–Cu mixed site *via* both  $C_1$  and  $C_2$  atoms; a Cu–C bond and two Co–C bonds are formed, and the corresponding adsorption energies are 176.3, 302.6 and 127.9  $\text{kJ mol}^{-1}$ , respectively.  $CH_2CHO$  adsorbs at the bridge-SE-2 Co–Cu mixed site *via* the  $C_1$ ,  $C_2$  and O atoms, and its adsorption energy is 279.8  $\text{kJ mol}^{-1}$ .  $CH_3COH$  adsorbs at the atop-SE Co site *via* the  $C_1$  atom with an adsorption energy of 303.3  $\text{kJ mol}^{-1}$ .

$CH_3CO$ ,  $CH_3CHO$  and  $CH_3CHOH$  adsorb favorably at the bridge-SE-2 Co–Cu mixed sites *via* both  $C_1$  and O atoms, and

the corresponding adsorption energies are 257.4, 129.5, and 201.6  $\text{kJ mol}^{-1}$ , respectively.  $CH_3CH_2O$  and  $CH_3CH_2OH$  are adsorbed *via* an O atom at the bridge-SE-2 Co–Cu mixed site and the atop-SE Co sites, and the corresponding adsorption energies are 290.9 and 68.9  $\text{kJ mol}^{-1}$ , respectively.

The above results show that after introducing the Co atom into the Cu catalyst, all species prefer to interact with Co atoms or the sites consisting of Co and Cu atoms rather than the Cu atoms, namely, the surface Co and Cu atoms of CoCu(211) are the active sites and exhibit a synergetic function between the active Co–Cu dual-sites for syngas conversion, which is in agreement with the previous experimental results.<sup>27,28</sup>

### 3.2 CO initial activation

CO initial activation is regarded as the initial key step for the formation of  $CH_x$  ( $x = 1-3$ ) intermediates in syngas conversion, which determines the formation pathway of  $CH_x$  ( $x = 1-3$ ) species; one is the direct C–O bond scission of CO into C and O atoms followed by C hydrogenation to  $CH_x$  species; the other is CO successive hydrogenation to  $CH_xO$  or  $CH_xOH$  intermediates followed by its direct or H-assisted C–O bond cleavage to form  $CH_x$  species.

For CO initial activation, since CO and  $H_2$ , as the initial reactants, are abundant surface species over the CoCu catalyst in the FTS reaction, CO is thought to be widely adsorbed

**Table 1** The adsorption energy (kJ mol<sup>-1</sup>) and key geometrical parameters (Å) of all possible intermediates involved in C<sub>2</sub> oxygenate and hydrocarbon formation from syngas

Species	$E_{\text{ads}}$	Configuration	Key parameters
C	677.1	Hollow-2	Co-C: 1.718; Cu-C: 1.926, 1.940, 1.961, 2.205
H-CoCu	252.9	Bridge-SE-2	Co-H: 1.583; Cu-H: 1.688
H-Cu	212.2	Fcc-SE-1	Cu-H: 1.724, 1.734, 1.743
O	577.4	Hcp-SE-2	Co-O: 1.730; Cu-O: 1.901, 2.047
OH	387.7	Bridge-SE-2	Co-O: 1.855; Cu-O: 1.990; O-H: 0.977
CO-Co	218.8	Atop-SE	Co-C: 1.725; C-O: 1.171
CO-Cu	89.5	Bridge-SE-1	Cu-C: 1.977, 1.979; C-O: 1.172
CH	593.5	Hollow-2	Co-C: 1.813; Cu-C: 2.033, 2.046, 2.101; C-H: 1.105
CH <sub>2</sub>	407.4	Bridge-SE-2	Co-C: 1.800; Cu-C: 2.042; C-H: 1.099, 1.105
CH <sub>3</sub>	221.3	Bridge-SE-2	Co-C: 1.956; Cu-C: 1.187; C-H: 1.103, 1.106, 1.120
CHO-CoCu	264.8	Bridge-SE-2 <i>via</i> C and O	Co-C: 1.814; Cu-O: 2.038; C-O: 1.257; C-H: 1.120
CHO-Cu	155.1	Bridge-SE-1 <i>via</i> C and O	Cu-C: 2.264; Cu-O: 2.235; C-O: 1.247; C-H: 1.117
CH <sub>2</sub> O	148.8	Bridge-SE-2 <i>via</i> C and O	Co-C: 1.956; Co-O: 1.910; Cu-O: 2.025; C-O: 1.352; C-H: 1.098, 1.099
CH <sub>3</sub> O	294.8	Bridge-SE-2 <i>via</i> O	Co-O: 1.841; Cu-O: 1.996; C-O: 1.436; C-H: 1.099, 1.101, 1.101
COH	386.2	Hcp-SE-2 <i>via</i> C	Co-C: 1.724; Cu-C: 1.968, 2.214; C-O: 1.328; O-H: 0.982
CHOH	323.4	Atop-SE <i>via</i> C	Co-C: 1.784; 1.354; C-H: 1.103; O-H: 0.981
CH <sub>2</sub> OH	213.3	Bridge-SE-2 <i>via</i> C and O	Co-C: 1.902; Cu-O: 2.124; C-O: 1.477; C-H: 1.097, 1.103; O-H: 0.977
CH <sub>3</sub> OH	71.3	Atop-SE <i>via</i> O	Co-O: 2.029; C-O: 1.454; C-H: 1.094, 1.098, 1.100; O-H: 0.976
H <sub>2</sub> O	63.7	Atop-SE <i>via</i> O	Co-O: 2.041; O-H: 0.978, 0.983
CH <sub>4</sub>	13.6	Away from surface	Co-C: 2.301; C-H: 1.095, 1.095, 1.122, 1.122
C <sub>2</sub> H <sub>4</sub>	139.9	Atop-SE <i>via</i> C <sub>1</sub> and C <sub>2</sub>	Co-C <sub>1</sub> : 2.018; Co-C <sub>2</sub> : 2.026; C-H: 1.094, 1.094, 1.094, 1.094
C <sub>2</sub> H <sub>6</sub>	24.0	Away from surface	Co-C <sub>1</sub> : 2.301; Cu-C <sub>2</sub> : 3.491; C <sub>1</sub> -H: 1.098, 1.099, 1.102; C <sub>2</sub> -H: 1.098, 1.127, 1.128
CH <sub>2</sub> CO	176.3	Bridge-SE-2 <i>via</i> C <sub>1</sub> <sup>a</sup> and C <sub>2</sub>	Co-C <sub>1</sub> : 1.770; Co-C <sub>2</sub> : 2.063; Cu-C <sub>2</sub> : 2.253; C <sub>1</sub> -O: 1.231; C <sub>2</sub> -H: 1.098, 1.098
CH <sub>2</sub> CO H	302.6	Bridge-SE-2 <i>via</i> C <sub>1</sub> and C <sub>2</sub>	Co-C <sub>1</sub> : 1.727; Co-C <sub>2</sub> : 2.138; Cu-C <sub>2</sub> : 2.171; C <sub>1</sub> -O: 1.326; C <sub>2</sub> -H: 1.097, 1.105; O-H: 0.985
CH <sub>2</sub> CHO	279.8	Bridge-SE-2 <i>via</i> C <sub>1</sub> , C <sub>2</sub> and O	Co-C <sub>1</sub> : 1.960; Co-C <sub>2</sub> : 2.122; Co-O: 2.058; Cu-O: 2.017; C <sub>1</sub> -O: 1.335; C <sub>1</sub> -H: 1.097; C <sub>2</sub> -H: 1.093, 1.099
CH <sub>2</sub> CHOH	127.9	Bridge-SE-2 <i>via</i> C <sub>1</sub> and C <sub>2</sub>	Co-C <sub>1</sub> : 1.982; Co-C <sub>2</sub> : 2.097; Cu-C <sub>2</sub> : 2.262; C <sub>1</sub> -O: 1.392; C <sub>1</sub> -H: 1.096; C <sub>2</sub> -H: 1.093, 1.100; O-H: 0.977
CH <sub>3</sub> CO	257.4	Bridge-SE-2 <i>via</i> C <sub>1</sub> and O	Co-C <sub>1</sub> : 1.808; Cu-O: 2.013; C <sub>1</sub> -O: 1.266; C <sub>2</sub> -H: 1.096, 1.101, 1.101
CH <sub>3</sub> COH	303.3	Atop-SE <i>via</i> C <sub>1</sub>	Co-C <sub>1</sub> : 1.783; C <sub>1</sub> -O: 1.348; C <sub>2</sub> -H: 1.094, 1.103, 1.103; O-H: 0.983
CH <sub>3</sub> CHO	129.5	Bridge-SE-2 <i>via</i> C <sub>1</sub> and O	Co-C <sub>1</sub> : 1.979; Co-O: 1.910; Cu-O: 2.019; C <sub>1</sub> -O: 1.353; C <sub>1</sub> -H: 1.100; C <sub>2</sub> -H: 1.098, 1.099, 1.105
CH <sub>3</sub> CHOH	201.6	Bridge-SE-2 <i>via</i> C <sub>1</sub> and O	Co-C <sub>1</sub> : 1.923; Cu-O: 2.126; C <sub>1</sub> -O: 1.479; C <sub>1</sub> -H: 1.099; C <sub>2</sub> -H: 1.099, 1.100, 1.105; O-H: 0.970
CH <sub>3</sub> CH <sub>2</sub> O	290.9	Bridge-SE-2 <i>via</i> O	Co-O: 1.833; Cu-O: 1.990; C <sub>1</sub> -O: 1.438; C <sub>1</sub> -H: 1.102, 1.103; C <sub>2</sub> -H: 1.099, 1.100, 1.100
C <sub>2</sub> H <sub>5</sub> OH	68.9	Atop-SE <i>via</i> O	Co-O: 2.005; C <sub>1</sub> -O: 1.463; C <sub>1</sub> -H: 1.099, 1.101; C <sub>2</sub> -H: 1.076, 1.100, 1.100; O-H: 0.975

<sup>a</sup> C<sub>1</sub> denotes the C atom linked with functional groups.

over the CoCu(211) surface including Cu and Co sites; in addition, CO adsorption reaches more than 0.5 ML (monolayer) on the Cu(100) surface<sup>80</sup> and the Co(0001) surface<sup>81</sup> under high temperature and pressure. As a result, CO initial activation over Cu and Co sites have been examined, and three possible reactions occur at the Co site of the CoCu(211) surface: CO direct dissociation (R1), CO hydrogenation to COH (R2) and CO hydrogenation to CHO (R3). Meanwhile, previous studies on the pure Cu(211) surface<sup>20</sup> have shown that CO hydrogenation to CHO at the Cu site is the most favorable; thus, CO hydrogenation to CHO (R4) at the Cu site of CoCu(211) and the diffusion of CHO species (R5) from the Cu site to the Co-Cu mixed site have also been considered. The potential energy diagram for the above five reactions together with the initial states (ISs), transition states (TSs) and final states (FSs) are shown in Fig. 3.

For R1, the direct C-O bond cleavage of CO adsorbed at the atop-SE Co site can form C and O *via* a transition state TS1; this elementary reaction requires an activation barrier of 387.4 kJ mol<sup>-1</sup> with the reaction energy of 129.9 kJ mol<sup>-1</sup> and the reaction rate constant is  $6.93 \times 10^{-28} \text{ s}^{-1}$  at 500 K (in the

main text, only the rate constants of all elementary reactions at the temperature of 500 K is presented, those at other temperatures are listed in Table 3); in TS1, C and O adsorb at the bridge-SE-2 Co-Cu site, and the C-O distance is elongated to 1.941 Å from 1.171 Å in CO.

When CO and H species are co-adsorbed at the Co-Cu mixed sites, for R2, CO hydrogenation can form COH *via* a transition state TS2; this elementary reaction has an activation barrier of 238.6 kJ mol<sup>-1</sup> with the reaction energy of 164.2 kJ mol<sup>-1</sup>, and the reaction rate constant is  $2.19 \times 10^{-12} \text{ s}^{-1}$ . In TS2, CO adsorbs at the bridge-SE-2 Co-Cu site, and the O-H distance is decreased to 1.254 Å from 2.991 Å in the initial state, CO + H(1); the final state COH is adsorbed *via* a C atom at the hcp-SE-2 Co-Cu mixed site. In R3, a H atom associating with a C atom of CO can form CHO *via* a transition state TS3, since the C-H distance in TS3 and the TS3 structure are also close to that of its product CHO, the energy of TS3 is similar to that of its product CHO. Thus, this elementary reaction is strongly endothermic by 108.9 kJ mol<sup>-1</sup> with an activation barrier of 112.7 kJ mol<sup>-1</sup>, and the reaction rate constant is  $3.80 \times 10^1 \text{ s}^{-1}$ . In TS3, the C-H distance is

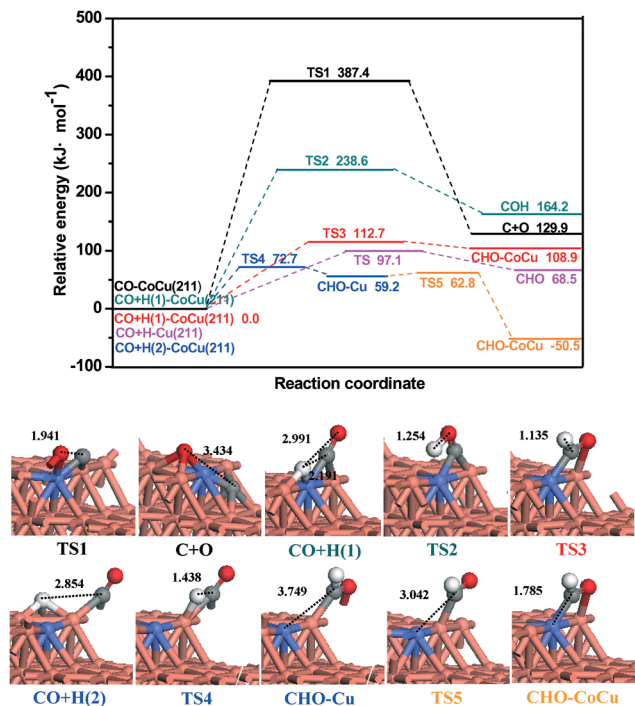


Fig. 3 The potential energy diagram of CO initial activation together with the structures of ISs, TSs and FSs. Bond lengths are in Å. See Fig. 2 for color coding.

decreased to 1.135 Å from 2.191 Å in the initial state, CO + H(1); the final state CHO is adsorbed *via* both C and O atoms at the bridge-SE-2 Co–Cu mixed site, which has an adsorption energy of 264.8 kJ mol<sup>-1</sup>. In addition, previous studies about CO hydrogenation to CHO on Co catalyst, such as Co(0001),<sup>82</sup> Co(211)<sup>83</sup> and Co(111)<sup>84</sup> surfaces, also have shown that the energy and structure of the transition state for CO hydrogenation to CHO is similar to that of the product CHO.

For R4, when CO and H species are co-adsorbed at the Cu sites, the bridge-SE-1 and fcc-SE-1 sites, respectively, CO hydrogenation to CHO only requires an activation barrier of 72.7 kJ mol<sup>-1</sup> with the reaction energy of 59.2 kJ mol<sup>-1</sup>, and the reaction rate constant is  $2.68 \times 10^5$  s<sup>-1</sup>. In TS4, CO and H species are adsorbed at the bridge-SE-2 Cu–Cu site and atop-SE Cu sites, respectively, and the C–H distance is decreased to 1.438 Å from 2.854 Å in the initial state, CO + H(2); moreover, CHO adsorbed at the bridge-SE-1 Cu–Cu mixed site has an adsorption energy of 154.1 kJ mol<sup>-1</sup>, which is less stable than that at the bridge-SE-2 Co–Cu mixed site with an adsorption energy of 264.8 kJ mol<sup>-1</sup>. As a result, CHO species will diffuse from the Cu site to the Co–Cu mixed site *via* TS5 in R5; this reaction has only a very small activation barrier of 3.6 kJ mol<sup>-1</sup>, and it is strongly exothermic by 109.7 kJ mol<sup>-1</sup>. In TS5, the Co–C distance is decreased to 3.042 Å from 3.749 Å.

As shown in Fig. 3, at the Co–Cu mixed site, among three possible reactions, although CO hydrogenation to CHO is the energetically favorable pathway, it is always highly endothermic. However, at the Cu site, CO hydrogenation to CHO is more favorable both thermodynamically and dynamically

than that at the Co–Cu mixed site, which is consistent with the previous studies.<sup>24</sup> CO hydrogenation to CHO at the Cu site has only an activation barrier of 72.7 kJ mol<sup>-1</sup>, which is also lower than that on the pure Cu(211) surface (97.1 kJ mol<sup>-1</sup>, 108.1<sup>20</sup> kJ mol<sup>-1</sup>), suggesting that the CoCu(211) surface is more favorable for CO hydrogenation to CHO than the pure Cu(211) surface. Subsequently, the diffusion of CHO species from the Cu site to the Co–Cu mixed site only has a very small activation barrier of 3.6 kJ mol<sup>-1</sup>, indicating that the facile diffusion of CHO species from the Cu site to the Co–Cu mixed site would increase the concentrations of CHO species at the Co–Cu mixed site.

In general, on the CoCu(211) surface, CO activation and hydrogenation to form CHO should go through three steps: firstly, CO and H species are co-adsorbed at the Cu sites; then, CO hydrogenation leads to CHO adsorption at the Cu site; this reaction has the largest rate constant of  $2.68 \times 10^5$  s<sup>-1</sup> among the different CO activation pathways. Further, CHO easily migrates from the Cu site to the most stable Co–Cu mixed site with the rate constant of  $1.58 \times 10^{13}$  s<sup>-1</sup>. With respect to the CO + H species, the overall reaction of CHO formation has the activation barrier and reaction energy of 72.7 and -50.5 kJ mol<sup>-1</sup>, respectively, which is more favorable than other formation pathways both thermodynamically and dynamically.

Therefore, the CHO species is the dominant product of CO initial activation on the CoCu(211) surface. Moreover, under the real experimental conditions, the abundant H on catalyst surface can facilitate CHO formation by CO hydrogenation. In fact, the CHO species has been accepted in many reactions related to CO hydrogenation. Deluzarche *et al.*<sup>85</sup> in their study on Rh/TiO<sub>2</sub> presented a plausible pathway to form ethanol from syngas *via* the CHO species. Experiments on Rh/SiO<sub>2</sub> catalysts containing CeO<sub>2</sub> (ref. 86) and Li-promoted Pd/CeO<sub>2</sub> (ref. 87) have shown the significance of the CHO species for alcohol synthesis using the chemical trapping approach. The studies by Remediakis *et al.* on Ni(111) surface<sup>88</sup> have indicated that the CHO species is an important intermediate involved in CH<sub>3</sub>OH formation from syngas.

### 3.3 CH<sub>x</sub> (x = 1–3) formation

In this section, the formation of CH<sub>x</sub> (x = 1–3) over the CoCu(211) surface have been examined; a detailed discussion about the elementary reactions involved in CH<sub>x</sub> (x = 1–3) formation are presented in the ESI.† Table 2 lists the activation barriers and reaction energies with the zero-point correction of all possible elementary reactions involved in the formation of CH<sub>x</sub>, C<sub>2</sub> oxygenates and hydrocarbons from syngas on the CoCu(211) surface.

**3.3.1 CH formation.** As mentioned above, CHO species adsorbed at the Co–Cu mixed site is the dominant product for CO initial activation on the CoCu(211) surface; thus, starting from CHO and CHO + H species, four possible pathways with five reactions (R6–R10) may be responsible for CH formation. Meanwhile, CHO hydrogenation to CH<sub>2</sub>O (R11) is also considered.

**Table 2** Possible elementary reactions involved in the formation of CH<sub>x</sub>, C<sub>2</sub> oxygenates and hydrocarbons from syngas together with the activation energies ( $E_a$ ) and reaction energies ( $\Delta E$ ) as well as the imaginary frequency (cm<sup>-1</sup>) corresponding to the transition state on the CoCu(211) surface

	Elementary reactions	Transition state (cm <sup>-1</sup> )	$E_a$ (kJ mol <sup>-1</sup> )	$\Delta E$ (kJ mol <sup>-1</sup> )
R1	CO → C + O	TS1 (497.0i)	387.4	129.9
R2	CO + H → COH	TS2 (1425.8i)	238.6	164.2
R3	CO + H → CHO-CoCu	TS3 (237.1i)	112.7	108.9
R4	CO + H → CHO-Cu	TS4 (426.9i)	72.7	59.2
R5	CHO-Cu → CHO-CoCu	TS5 (228.5i)	3.6	-109.7
R6	CHO → CH + O	TS6 (478.0i)	169.2	-0.1
R7	CHO + H → CH + OH	TS7 (377.9i)	155.7	12.9
R8	CHO + H → CHOH	TS8 (1457.1i)	133.0	55.1
R9	CHOH → CH + OH	TS9 (378.9i)	102.0	-42.2
R10	CHOH + H → CH + H <sub>2</sub> O	TS10 (1332.2i)	188.1	25.2
R11	CHO + H → CH <sub>2</sub> O	TS11 (293.1i)	47.7	3.3
R12	CHO + H → CH <sub>2</sub> + O	—	—	—
R13	CH <sub>2</sub> O → CH <sub>2</sub> + O	TS13 (448.0i)	126.7	9.7
R14	CH <sub>2</sub> O + H → CH <sub>2</sub> + OH	TS14 (423.4i)	96.2	9.5
R15	CH <sub>2</sub> O + H → CH <sub>2</sub> OH	TS15 (1208.6i)	108.3	46.3
R16	CH <sub>2</sub> OH → CH <sub>2</sub> + OH	TS16 (426.0i)	51.3	-36.8
R17	CH <sub>2</sub> OH + H → CH <sub>2</sub> + H <sub>2</sub> O	TS17 (716.9i)	128.8	-7.6
R18	CH <sub>2</sub> O + H → CH <sub>3</sub> O	TS18 (624.7i)	29.2	3.4
R19	CH <sub>2</sub> O + H → CH <sub>3</sub> + O	TS19 (532.4i)	110.6	-12.3
R20	CH <sub>3</sub> O → CH <sub>3</sub> + O	TS20 (558.2i)	111.5	-15.7
R21	CH <sub>3</sub> O + H → CH <sub>3</sub> + OH	TS21 (385.3i)	92.8	-30.5
R22	CH <sub>3</sub> O + H → CH <sub>3</sub> OH	TS22 (1173.7i)	103.5	45.1
R23	CH <sub>2</sub> → CH + H	TS23 (729.0i)	41.1	5.8
R24	CH <sub>2</sub> + H → CH <sub>3</sub>	TS24 (797.2i)	19.0	-25.6
R25	CH <sub>2</sub> + CH <sub>2</sub> → C <sub>2</sub> H <sub>4</sub>	TS25 (43.3i)	17.7	-104.5
R26	CH <sub>2</sub> + CO → CH <sub>2</sub> CO	TS26 (384.9i)	39.9	12.1
R27	CH <sub>2</sub> + CHO → CH <sub>2</sub> CHO	TS27 (250.6i)	24.7	-91.9
R28	CH <sub>3</sub> → CH <sub>2</sub> + H	TS28 (797.2i)	44.6	25.6
R29	CH <sub>3</sub> + H → CH <sub>4</sub>	TS29 (624.9i)	87.3	-0.2
R30	CH <sub>3</sub> + CH <sub>3</sub> → C <sub>2</sub> H <sub>6</sub>	TS30 (181.5i)	156.2	-39.4
R31	CH <sub>3</sub> + CO → CH <sub>3</sub> CO	TS31 (397.4i)	83.1	30.4
R32	CH <sub>3</sub> + CHO → CH <sub>3</sub> CHO	TS32 (272.2i)	41.1	-66.8
R33	CH <sub>3</sub> CO + H → CH <sub>3</sub> CO	TS33 (704.8i)	53.0	13.6
R34	CH <sub>2</sub> CO + H → CH <sub>2</sub> CHO	TS34 (440.6i)	59.4	-0.5
R35	CH <sub>2</sub> CO + H → CH <sub>2</sub> COH	TS35 (1371.4i)	128.6	69.1
R36	CH <sub>2</sub> CHO + H → CH <sub>3</sub> CHO	TS36 (642.9i)	42.9	0.1
R37	CH <sub>2</sub> CHO + H → CH <sub>2</sub> CHOH	TS37 (1238.7i)	94.9	41.4
R38	CH <sub>3</sub> CO + H → CH <sub>3</sub> CHO	TS38 (372.4i)	57.1	-14.0
R39	CH <sub>3</sub> CO + H → CH <sub>3</sub> CO H	TS39 (1384.9i)	123.8	58.7
R40	CH <sub>3</sub> CHO + H → CH <sub>3</sub> CH <sub>2</sub> O	TS40 (658.7i)	27.5	10.4
R41	CH <sub>3</sub> CHO + H → CH <sub>3</sub> CHOH	TS41 (1203.1i)	112.8	57.1
R42	CH <sub>3</sub> CH <sub>2</sub> O + H → C <sub>2</sub> H <sub>5</sub> OH	TS42 (1000.9i)	109.6	48.6

As illustrated in Fig. 4, among CH formation pathways, two parallel pathways, CHO + H → CH + OH and CHO + H → CHOH → CH + OH, are more favorable dynamically than the other two pathways; with respect to CHO + H species at the Co-Cu mixed site; both parallel pathways have the highest barriers of 155.7 and 157.1 kJ mol<sup>-1</sup>, respectively, and the corresponding reaction energy is 12.9 kJ mol<sup>-1</sup>. Meanwhile, the rate-determining steps of both parallel pathways are CHO + H → CH + OH and CHO + H → CHOH with the rate constants of  $8.14 \times 10^{-4}$  and  $0.36 \text{ s}^{-1}$ , respectively. As a result, the most favorable pathway of CH formation is CHO + H → CHOH → CH + OH.

However, CHO hydrogenation to CH<sub>2</sub>O has only an activation barrier of 47.7 kJ mol<sup>-1</sup>, and the rate constant is  $7.14 \times 10^8 \text{ s}^{-1}$ , which is much more favorable than that of CH formation, suggesting that the CHO species adsorbed at the Co-Cu

mixed site prefers to be hydrogenated to CH<sub>2</sub>O rather than being hydrogenated to CHOH and being dissociated into CH, respectively. Thus, the preferred products from CHO species should be CH<sub>2</sub>O at the Co-Cu mixed site.

**3.3.2 CH<sub>2</sub> formation.** As mentioned above, CH<sub>2</sub>O species adsorbed at the Co-Cu mixed sites is the preferred product from CHO species; as a result, starting from the initial state CHO + H, CH<sub>2</sub>O and CH<sub>2</sub>O + H species, five possible pathways with six reactions (R12–R17) lead to CH<sub>2</sub> formation. Our results show that for R12 (CHO + H → CH<sub>2</sub> + O), CHO prefers to be hydrogenated to CH<sub>2</sub>O, followed by dissociation into CH<sub>2</sub> and O. Meanwhile, CH<sub>2</sub>O hydrogenation to CH<sub>3</sub>O (R18) has been considered.

As presented in Fig. 5, among five possible pathways of CH<sub>2</sub> formation, H-assisted CH<sub>2</sub>O dissociation (R14) and *via* a CH<sub>2</sub>OH intermediate (R15 and R16) are two parallel

**Table 3** The rate constant  $k$  ( $s^{-1}$ ) for elementary reactions involved in the formation of  $CH_x$ ,  $C_2$  oxygenates and hydrocarbons from syngas at different temperatures on the CoCu(211) surface

	Elementary reactions	Rate constant $k$ ( $s^{-1}$ )				
		500 K	525 K	550 K	575 K	600 K
R1	CO → C + O	$6.93 \times 10^{-28}$	$6.18 \times 10^{-26}$	$3.72 \times 10^{-24}$	$1.58 \times 10^{-22}$	$4.89 \times 10^{-21}$
R2	CO + H → COH	$2.19 \times 10^{-12}$	$2.49 \times 10^{-11}$	$4.34 \times 10^{-10}$	$4.35 \times 10^{-9}$	$3.60 \times 10^{-8}$
R3	CO + H → CHO-CoCu	$3.80 \times 10^1$	$1.45 \times 10^2$	$4.89 \times 10^2$	$1.49 \times 10^3$	$4.151 \times 10^3$
R4	CO + H → CHO-Cu	$2.68 \times 10^5$	$8.50 \times 10^5$	$1.45 \times 10^6$	$4.06 \times 10^6$	$5.94 \times 10^6$
R5	CHO-Cu → CHO-CoCu	$1.58 \times 10^{13}$	$1.75 \times 10^{13}$	$1.94 \times 10^{13}$	$2.13 \times 10^{13}$	$2.32 \times 10^{13}$
R6	CHO → CH + O	$5.73 \times 10^{-6}$	$4.15 \times 10^{-5}$	$2.51 \times 10^{-4}$	$1.31 \times 10^{-3}$	$5.94 \times 10^{-3}$
R7	CHO + H → CH + OH	$8.14 \times 10^{-4}$	$5.20 \times 10^{-3}$	$2.81 \times 10^{-2}$	0.13	0.54
R8	CHO + H → CHOH	0.36	1.72	7.21	$2.67 \times 10^1$	$8.90 \times 10^1$
R9	CHOH → CH + OH	$2.03 \times 10^2$	$7.01 \times 10^2$	$2.17 \times 10^3$	$6.10 \times 10^3$	$1.58 \times 10^4$
R10	CHOH + H → CH + H <sub>2</sub> O	$2.76 \times 10^{-7}$	$2.52 \times 10^{-6}$	$1.89 \times 10^{-5}$	$1.19 \times 10^{-4}$	$6.46 \times 10^{-4}$
R11	CHO + H → CH <sub>2</sub> O	$7.14 \times 10^8$	$1.31 \times 10^9$	$2.27 \times 10^9$	$3.76 \times 10^9$	$5.98 \times 10^9$
R12	CHO + H → CH <sub>2</sub> + O	—	—	—	—	—
R13	CH <sub>2</sub> O → CH <sub>2</sub> + O	0.89	4.06	$1.62 \times 10^1$	$5.76 \times 10^1$	$1.84 \times 10^2$
R14	CH <sub>2</sub> O + H → CH <sub>2</sub> + OH	$1.88 \times 10^3$	$6.11 \times 10^3$	$1.79 \times 10^4$	$4.81 \times 10^4$	$1.19 \times 10^5$
R15	CH <sub>2</sub> O + H → CH <sub>2</sub> OH	$2.03 \times 10^2$	$7.49 \times 10^2$	$2.45 \times 10^3$	$7.26 \times 10^3$	$1.97 \times 10^4$
R16	CH <sub>2</sub> OH → CH <sub>2</sub> + OH	$3.17 \times 10^7$	$6.09 \times 10^7$	$1.10 \times 10^8$	$1.91 \times 10^8$	$3.15 \times 10^8$
R17	CH <sub>2</sub> OH + H → CH <sub>2</sub> + H <sub>2</sub> O	0.93	4.35	$1.78 \times 10^1$	$6.47 \times 10^1$	$2.12 \times 10^2$
R18	CH <sub>2</sub> O + H → CH <sub>3</sub> O	$2.92 \times 10^{10}$	$4.27 \times 10^{10}$	$6.06 \times 10^{10}$	$8.34 \times 10^{10}$	$1.12 \times 10^{11}$
R19	CH <sub>3</sub> O → CH <sub>3</sub> + O	6.22	$2.79 \times 10^1$	$1.10 \times 10^2$	$3.83 \times 10^2$	$1.21 \times 10^3$
R20	CH <sub>3</sub> O → CH <sub>3</sub> + O	$4.08 \times 10^2$	$1.33 \times 10^3$	$3.94 \times 10^3$	$1.06 \times 10^4$	$2.64 \times 10^3$
R21	CH <sub>3</sub> O + H → CH <sub>3</sub> + OH	$8.95 \times 10^3$	$2.82 \times 10^4$	$8.01 \times 10^4$	$2.08 \times 10^5$	$5.03 \times 10^5$
R22	CH <sub>3</sub> O + H → CH <sub>3</sub> OH	$5.01 \times 10^2$	$1.75 \times 10^3$	$5.44 \times 10^3$	$1.54 \times 10^4$	$4.00 \times 10^4$
R23	CH <sub>2</sub> → CH + H	$1.93 \times 10^8$	$3.23 \times 10^8$	$5.16 \times 10^8$	$7.95 \times 10^8$	$1.18 \times 10^9$
R24	CH <sub>2</sub> + H → CH <sub>3</sub>	$6.09 \times 10^{10}$	$7.90 \times 10^{10}$	$1.00 \times 10^{11}$	$1.25 \times 10^{11}$	$1.53 \times 10^{11}$
R25	CH <sub>2</sub> + CH <sub>2</sub> → C <sub>2</sub> H <sub>4</sub>	$1.96 \times 10^{11}$	$2.55 \times 10^{11}$	$3.23 \times 10^{11}$	$4.02 \times 10^{11}$	$4.93 \times 10^{11}$
R26	CH <sub>2</sub> + CO → CH <sub>2</sub> CO	$9.07 \times 10^8$	$1.49 \times 10^9$	$2.35 \times 10^9$	$3.56 \times 10^9$	$5.22 \times 10^9$
R27	CH <sub>2</sub> + CHO → CH <sub>2</sub> CHO	$4.30 \times 10^{10}$	$5.89 \times 10^{10}$	$7.87 \times 10^{10}$	$1.03 \times 10^{11}$	$1.31 \times 10^{11}$
R28	CH <sub>3</sub> → CH <sub>2</sub> + H	$5.45 \times 10^7$	$9.43 \times 10^7$	$1.56 \times 10^8$	$2.47 \times 10^8$	$3.78 \times 10^8$
R29	CH <sub>3</sub> + H → CH <sub>4</sub>	$3.23 \times 10^4$	$9.49 \times 10^4$	$2.54 \times 10^5$	$6.24 \times 10^5$	$1.42 \times 10^6$
R30	CH <sub>3</sub> + CH <sub>3</sub> → C <sub>2</sub> H <sub>6</sub>	$2.41 \times 10^{-2}$	0.16	0.93	4.56	$1.97 \times 10^1$
R31	CH <sub>3</sub> + CO → CH <sub>3</sub> CO	$1.30 \times 10^5$	$3.55 \times 10^5$	$8.90 \times 10^5$	$2.06 \times 10^6$	$4.46 \times 10^6$
R32	CH <sub>3</sub> + CHO → CH <sub>3</sub> CHO	$3.56 \times 10^9$	$6.01 \times 10^9$	$9.69 \times 10^9$	$1.50 \times 10^{10}$	$2.24 \times 10^{10}$
R33	CH <sub>2</sub> CO + H → CH <sub>3</sub> CO	$4.67 \times 10^7$	$9.02 \times 10^7$	$1.64 \times 10^8$	$2.85 \times 10^8$	$4.72 \times 10^8$
R34	CH <sub>2</sub> CO + H → CH <sub>2</sub> CHO	$3.11 \times 10^6$	$6.38 \times 10^6$	$1.23 \times 10^7$	$2.24 \times 10^7$	$3.89 \times 10^7$
R35	CH <sub>2</sub> CO + H → CH <sub>2</sub> CO H	3.04	$1.41 \times 10^1$	$5.68 \times 10^1$	$2.04 \times 10^2$	$6.58 \times 10^2$
R36	CH <sub>2</sub> CHO + H → CH <sub>3</sub> CHO	$1.36 \times 10^{10}$	$2.36 \times 10^{10}$	$3.91 \times 10^{10}$	$6.20 \times 10^{10}$	$9.49 \times 10^{10}$
R37	CH <sub>2</sub> CHO + H → CH <sub>2</sub> CHOH	$1.84 \times 10^3$	$5.76 \times 10^3$	$1.63 \times 10^4$	$4.23 \times 10^4$	$1.02 \times 10^5$
R38	CH <sub>3</sub> CO + H → CH <sub>3</sub> CHO	$1.16 \times 10^8$	$2.36 \times 10^8$	$4.52 \times 10^8$	$8.19 \times 10^8$	$1.42 \times 10^9$
R39	CH <sub>3</sub> CO + H → CH <sub>3</sub> CO H	6.81	$2.97 \times 10^1$	$1.13 \times 10^2$	$3.86 \times 10^2$	$1.19 \times 10^3$
R40	CH <sub>3</sub> CHO + H → CH <sub>3</sub> CH <sub>2</sub> O	$6.43 \times 10^{10}$	$9.34 \times 10^{10}$	$1.31 \times 10^{11}$	$1.80 \times 10^{11}$	$2.40 \times 10^{11}$
R41	CH <sub>3</sub> CHO + H → CH <sub>2</sub> CHOH	$1.29 \times 10^2$	$5.01 \times 10^2$	$1.72 \times 10^3$	$5.32 \times 10^3$	$1.50 \times 10^4$
R42	CH <sub>3</sub> CH <sub>2</sub> O + H → C <sub>2</sub> H <sub>5</sub> OH	$5.16 \times 10^2$	$1.93 \times 10^3$	$6.43 \times 10^3$	$1.93 \times 10^4$	$5.3 \times 10^4$

pathways; with respect to CHO + H species at the Co-Cu mixed site, both pathways have the highest barriers of 99.5 and 111.6 kJ mol<sup>-1</sup>, respectively. Meanwhile, the rate-determining steps of both parallel pathways are CH<sub>2</sub>O + H → CH<sub>2</sub> + OH and CH<sub>2</sub>O + H → CH<sub>2</sub>OH with the rate constants of  $1.88 \times 10^3$  and  $2.03 \times 10^2$  s<sup>-1</sup>, respectively. As a result, the most favorable pathway of CH<sub>2</sub> formation is CH<sub>2</sub>O + H → CH<sub>2</sub> + OH.

However, CH<sub>2</sub>O hydrogenation to CH<sub>3</sub>O has the reaction energy of 3.4 kJ mol<sup>-1</sup> with an activation barrier of 29.2 kJ mol<sup>-1</sup>, and the rate constant of this reaction is  $2.92 \times 10^{10}$  s<sup>-1</sup>, which is much more favorable than that of CH<sub>2</sub> formation and CH<sub>2</sub>O hydrogenation to CH<sub>2</sub>OH with the activation barrier of 108.3 kJ mol<sup>-1</sup>. Moreover, CH<sub>2</sub>O over the CoCu(211) surface has a strong adsorption energy of 148.8 kJ mol<sup>-1</sup>, in-

dicating that CH<sub>2</sub>O prefers to be hydrogenated to CH<sub>3</sub>O rather than being hydrogenated to CH<sub>2</sub>OH and being dissociated into CH<sub>2</sub> as well as CH<sub>2</sub>O being desorbed from the surface, respectively. Therefore, CH<sub>3</sub>O is more likely to be the preferred intermediate formed by CH<sub>2</sub>O hydrogenation.

**3.3.3 CH<sub>3</sub> and CH<sub>3</sub>OH formation.** Similarly, starting from CH<sub>2</sub>O + H, CH<sub>3</sub>O and CH<sub>3</sub>O + H species, three possible pathways (R19–R21) are responsible for CH<sub>3</sub> formation. CH<sub>3</sub>O hydrogenation to CH<sub>3</sub>OH (R22) has also been considered.

As illustrated in Fig. 6, among three pathways of CH<sub>3</sub> formation, H-assisted CH<sub>3</sub>O dissociation (R21) is predominantly responsible for CH<sub>3</sub> formation; this elementary reaction is exothermic by 30.5 kJ mol<sup>-1</sup> with an activation barrier of 92.8 kJ mol<sup>-1</sup>, and the corresponding rate constant is  $8.95 \times 10^3$  s<sup>-1</sup>, which is favorable both thermodynamically and

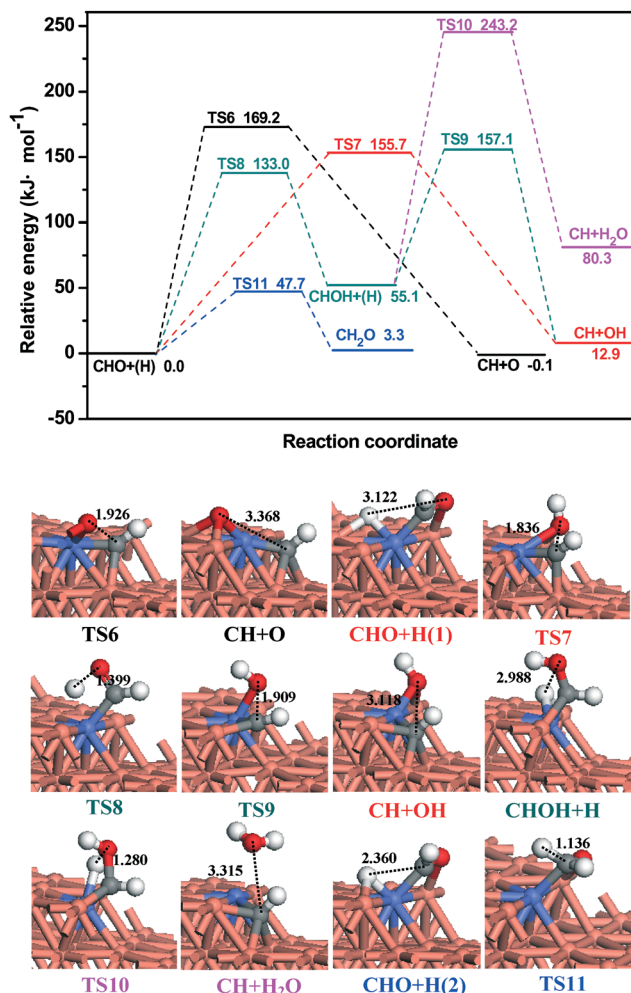


Fig. 4 The potential energy diagram for the formation of CH and  $\text{CH}_2\text{O}$  together with the structures of ISs, TSs and FSs. Bond lengths are in Å. See Fig. 2 for color coding.

kinetically than  $\text{CH}_3\text{O}$  hydrogenation to  $\text{CH}_3\text{OH}$  (R22) with the activation barrier and reaction energy of 103.5 and 45.1  $\text{kJ mol}^{-1}$ , respectively, and a rate constant of  $5.01 \times 10^2 \text{ s}^{-1}$ .

### 3.4 The most favorable $\text{CH}_x$ ( $x = 1-3$ ) monomer and $\text{CH}_3\text{OH}$ formation

Starting from  $\text{CHO} + \text{H}$  adsorbed at the Co–Cu mixed sites, Fig. 7 presents the potential energy diagram for the most favorable formation pathways of  $\text{CH}_x$  ( $x = 1-3$ ) species and  $\text{CH}_3\text{OH}$ .

For CH formation,  $\text{CHO} + \text{H} \rightarrow \text{CHOH} \rightarrow \text{CH} + \text{OH}$  is the most favorable pathway with the highest barriers and reaction energy of 157.1 and 12.9  $\text{kJ mol}^{-1}$ , respectively, and the rate-determining step is  $\text{CHO} + \text{H} \rightarrow \text{CHOH}$ , which has the rate constant of  $0.36 \text{ s}^{-1}$ .

For  $\text{CH}_2$  formation, the most favorable pathway is  $\text{CHO} + \text{H} \rightarrow \text{CH}_2\text{O} + \text{H} \rightarrow \text{CH}_2 + \text{OH}$ , which has the highest barrier and reaction energy of 99.5 and 12.8  $\text{kJ mol}^{-1}$ , respectively;  $\text{CH}_2\text{O} + \text{H} \rightarrow \text{CH}_2 + \text{OH}$  is the rate-determining step with the rate constant of  $1.88 \times 10^3 \text{ s}^{-1}$ .

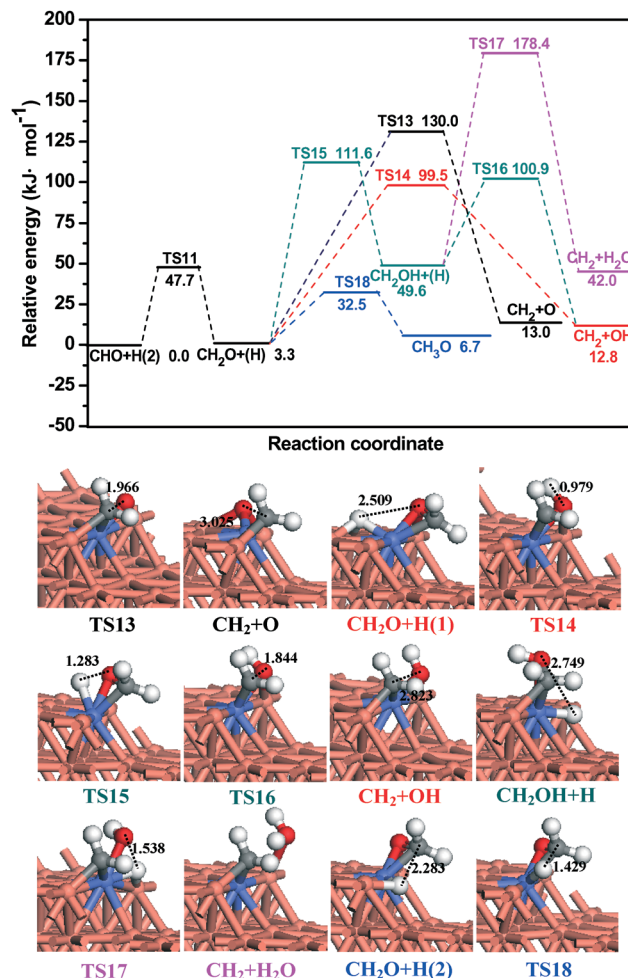


Fig. 5 The potential energy diagram for the formation of  $\text{CH}_2$  and  $\text{CH}_3\text{O}$  together with the structures of ISs, TSs and FSs. Bond lengths are in Å. See Fig. 2 for color coding.

For  $\text{CH}_3$  formation, the pathway of  $\text{CHO} + \text{H} \rightarrow \text{CH}_2\text{O} + \text{H} \rightarrow \text{CH}_3\text{O} \rightarrow \text{CH}_3 + \text{OH}$  has the highest barrier and reaction energy of 99.5 and  $-23.8 \text{ kJ mol}^{-1}$ , respectively;  $\text{CH}_3\text{O} + \text{H} \rightarrow \text{CH}_3 + \text{OH}$  is the rate-determining step with the rate constant of  $8.95 \times 10^3 \text{ s}^{-1}$ .

For  $\text{CH}_3\text{OH}$  formation, the pathway of  $\text{CHO} + \text{H} \rightarrow \text{CH}_2\text{O} + \text{H} \rightarrow \text{CH}_3\text{O} + \text{H} \rightarrow \text{CH}_3\text{OH}$  has the highest barrier and reaction energy of 110.2 and 51.8  $\text{kJ mol}^{-1}$ , respectively;  $\text{CH}_3\text{O} + \text{H} \rightarrow \text{CH}_3\text{OH}$  is the rate-determining step with the rate constant of  $5.01 \times 10^2 \text{ s}^{-1}$ .

The above results show that  $\text{CH}_2$  and  $\text{CH}_3$  species are the most favorable monomers among all  $\text{CH}_x$  ( $x = 1-3$ ) species; moreover, the formation of  $\text{CH}_2$  and  $\text{CH}_3$  species is favorable both thermodynamically and kinetically than  $\text{CH}_3\text{OH}$  formation, which means that the CoCu(211) surface exhibits good selectivity toward the formation of  $\text{CH}_2$  and  $\text{CH}_3$  species rather than  $\text{CH}_3\text{OH}$  in syngas conversion.

On the other hand,  $\text{CH}_x$  formation *via* H-assisted CO dissociation is also much more favorable than that *via* CO direct dissociation with an activation barrier of 387.4  $\text{kJ mol}^{-1}$ , namely,  $\text{CH}_x$  species is predominantly formed *via* the

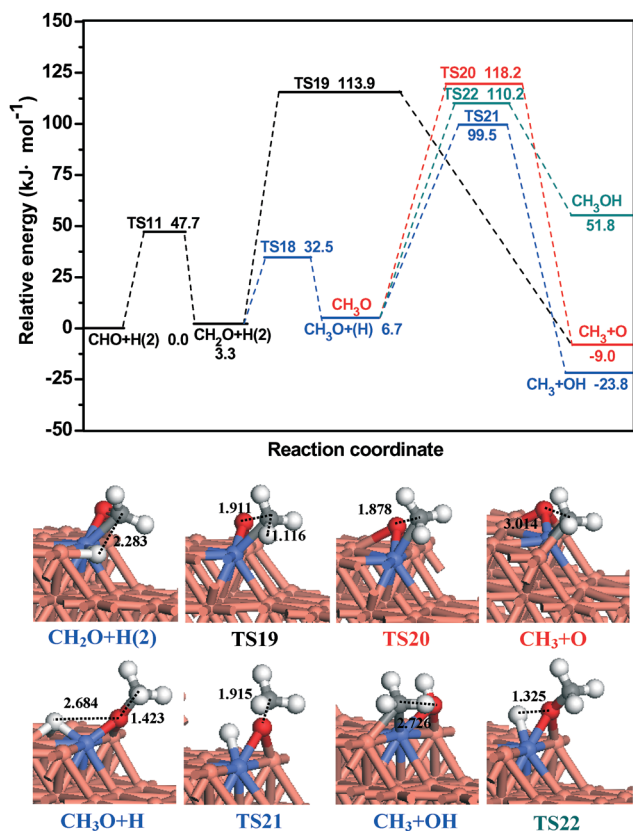


Fig. 6 The potential energy diagram for the formation of  $\text{CH}_3$  and  $\text{CH}_3\text{OH}$  together with the structures of ISs, TSs and FSs. Bond lengths are in Å. See Fig. 2 for color coding.

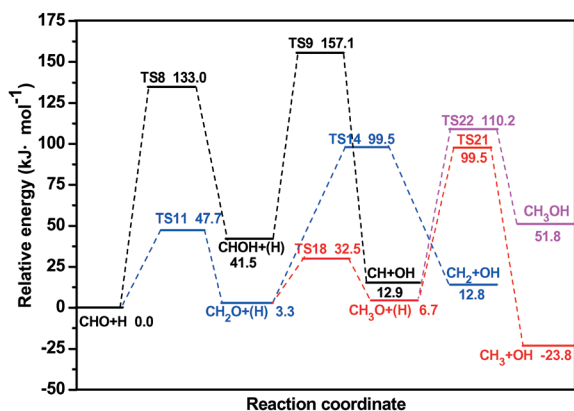


Fig. 7 The potential energy diagram for the most favorable pathway of  $\text{CH}_x$  ( $x = 1-3$ ) and  $\text{CH}_3\text{OH}$  formation.

mechanism of H-assisted CO dissociation over the CoCu(211) surface rather than CO direct dissociation into O and C followed by C hydrogenation.

Our previous DFT studies about syngas conversion on the pure Cu(211) surface<sup>20</sup> have suggested that  $\text{CH}_3$  species is the most favorable monomer; however,  $\text{CH}_3\text{OH}$  formation is much more favorable than  $\text{CH}_3$  species formation, which agrees with the general fact that Cu catalyst shows good cata-

lytic performance for  $\text{CH}_3\text{OH}$  formation from syngas. Clearly, upon Co doping with Cu, since the Co-based catalyst is in favor of  $\text{CH}_x$  formation from syngas, the selectivity to  $\text{CH}_x$  ( $x = 2, 3$ ) species is improved significantly over the Co-decorated Cu-based catalyst due to the synergetic effect between the active Co-Cu dual sites. Therefore, compared to the pure Cu(211) surface, the CoCu(211) surface can provide more  $\text{CH}_x$  resources for further C-C chain formation in syngas conversion.

### 3.5 The formation of $\text{C}_2$ hydrocarbons and oxygenates

On the basis of the above results,  $\text{CH}_2$  and  $\text{CH}_3$  monomers are the dominant existing form of  $\text{CH}_x$  ( $x = 1-3$ ) species from syngas on Co-decorated Cu(211) surface; moreover, in syngas conversion, since the catalyst surface is covered by certain amounts of hydrogen under realistic reaction conditions, the formation channel of  $\text{CH}_x$  upon hydrogenation should be involved. Thereby, based on the most favorable  $\text{CH}_2$  and  $\text{CH}_3$  monomers,  $\text{CH}_2$  hydrogenation could act as an alternative route for  $\text{CH}_3$  formation. In summary, once the  $\text{CH}_x$  monomer is formed, C-C chain formation starts immediately, and this process will be presented in the following part.

Starting from the most favorable  $\text{CH}_x$  monomers,  $\text{CH}_2$  and  $\text{CH}_3$  species, all possible reactions related to  $\text{CH}_2$  and  $\text{CH}_3$  species, including the dissociation, hydrogenation, coupling and CO/CHO insertion, have been examined, in which a detailed discussion about the elementary reactions are presented in the ESI.† Fig. 8 and 9 present the potential energy profile of these reactions related to  $\text{CH}_2$  and  $\text{CH}_3$  species together with the corresponding structures, respectively.

As shown in Fig. 8, among all reactions related to  $\text{CH}_2$  species,  $\text{CH}_2$  coupling to  $\text{C}_2\text{H}_4$  (R25) is the most favorable kinetically, which has only an activation barrier of 17.7  $\text{kJ mol}^{-1}$  with the reaction energy of  $-104.5 \text{ kJ mol}^{-1}$ . Meanwhile,  $\text{CH}_2$  hydrogenation to  $\text{CH}_3$  (R24) has an activation barrier of 19.0  $\text{kJ mol}^{-1}$ , which is competitive with  $\text{CH}_2$  coupling.  $\text{CH}_2$  dissociation (R23) and CO insertion into  $\text{CH}_2$  (R26) have the activation barriers of 41.1 and 39.9  $\text{kJ mol}^{-1}$  with the corresponding reaction energies of 5.8 and 12.1  $\text{kJ mol}^{-1}$ , respectively. CHO insertion into  $\text{CH}_2$  to  $\text{CH}_2\text{CHO}$  (R27) has the highest barrier of 72.7  $\text{kJ mol}^{-1}$ , which is less favorable than CO insertion into  $\text{CH}_2$ . Based on the kinetic data,  $\text{CH}_2$  coupling to  $\text{C}_2\text{H}_4$  and  $\text{CH}_2$  hydrogenation to  $\text{CH}_3$  have a small difference in activation barrier. However, previous results<sup>89</sup> have suggested that the saturated coverage of H is 6/12 ML (monolayer) on the Rh (100) surface, and the coverage of  $\text{H}_2$  can reach 0.3 ML (monolayer)<sup>90</sup> on the Co(0001) surface in the presence of 1/3 ML (monolayer) CO in the F-T synthesis process. As a result, under realistic conditions,  $\text{CH}_2$  hydrogenation is much faster than  $\text{CH}_2$  coupling and  $\text{CH}_2$  dissociation due to the abundant existence of hydrogen. On the other hand, CO is also considered as an abundant surface intermediate in syngas conversion, for example, CO adsorption reaches 0.5 ML (monolayer) on the Cu(100) surface<sup>80</sup> and the Co(0001) surface<sup>81</sup> under high temperature and pressure. Theoretical calculations<sup>91</sup> have also proved

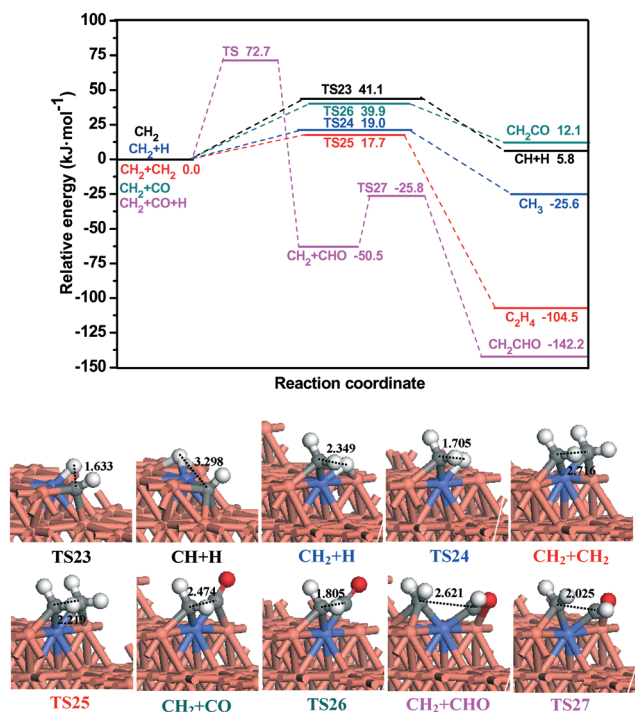


Fig. 8 The potential energy diagram of the reactions related to  $\text{CH}_2$  species together with the structures of ISs, TSs and FSs. Bond lengths are in Å. See Fig. 2 for color coding.

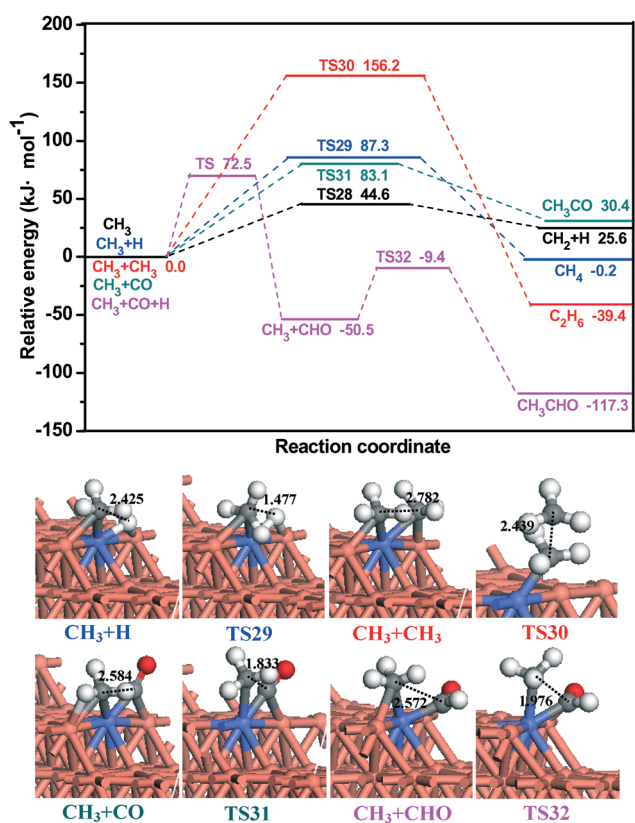


Fig. 9 The potential energy diagram of the reactions related to  $\text{CH}_3$  species together with the structures of ISs and TSs. Bond lengths are in Å. See Fig. 2 for color coding.

that the coverage ratio of CO to CHO is  $10^6$  times under typical F–T conditions. Thus, although  $\text{CH}_2$  coupling is faster than the CO insertion reaction in kinetics, CO insertion into  $\text{CH}_2$  to  $\text{C}_2$  oxygenate  $\text{CH}_2\text{CO}$  can be accelerated due to the abundant coverage of CO, and it is also faster than CHO insertion into  $\text{CH}_2$  and  $\text{CH}_2$  coupling, which is consistent with the previous studies.<sup>92</sup> Eventually,  $\text{CH}_3$  and  $\text{C}_2$  oxygenate  $\text{CH}_2\text{CO}$  should be the major products among the reactions related to  $\text{CH}_2$  species.

Similarly, as shown in Fig. 9, among all reactions related to  $\text{CH}_3$  species,  $\text{CH}_3$  dissociation (R28) has the lowest barrier of  $44.6 \text{ kJ mol}^{-1}$  followed by CHO and CO insertion into  $\text{CH}_3$  to  $\text{CH}_3\text{CHO}$  (R32) and  $\text{CH}_3\text{CO}$  (R31) as well as  $\text{CH}_3$  hydrogenation to  $\text{CH}_4$  (R29) with the activation barriers of  $72.7$ ,  $83.1$ , and  $87.3 \text{ kJ mol}^{-1}$ , respectively.  $\text{CH}_3$  coupling (R30) is difficult to occur due to the high activation barrier of  $156.2 \text{ kJ mol}^{-1}$ . Similar to  $\text{CH}_2$  species, starting from  $\text{CH}_3$  species,  $\text{CH}_3$  hydrogenation to  $\text{CH}_4$  is faster than  $\text{CH}_3$  dissociation owing to the abundant coverage of hydrogen. Meanwhile, CO insertion into  $\text{CH}_3$  to  $\text{CH}_3\text{CO}$  is accelerated due to the abundant coverage of CO; CO insertion is faster than CHO insertion, in which CHO predominantly contributes to  $\text{CH}_x$  ( $x = 2, 3$ ) species formation *via* the intermediates  $\text{CH}_2\text{O}$  and  $\text{CH}_3\text{O}$ . Thus, among the reactions related to  $\text{CH}_3$  species,  $\text{C}_2$  oxygenate  $\text{CH}_3\text{CO}$  should be the major product followed by  $\text{CH}_4$ .

On the basis of the above analysis, starting from  $\text{CH}_2$  and  $\text{CH}_3$  species, the CoCu(211) surface exhibits a better selectivity toward the formation of  $\text{C}_2$  oxygenates  $\text{CH}_2\text{CO}$  and  $\text{CH}_3\text{CO}$ , and  $\text{CH}_4$  is formed as the by-product. Then,  $\text{CH}_2\text{CO}$  and  $\text{CH}_3\text{CO}$  can be successively hydrogenated to  $\text{C}_2\text{H}_5\text{OH}$ . A detailed discussion about the elementary reactions involved in  $\text{C}_2\text{H}_5\text{OH}$  formation is presented in the ESI.† Starting from  $\text{CH}_2\text{CO}$  species, Fig. 10 presents the potential energy profile of ethanol formation together with the structures of ISs and TSs.

As shown in Fig. 10, starting from  $\text{CH}_2\text{CO}$ ,  $\text{CH}_2\text{CO}$  hydrogenation to  $\text{CH}_2\text{CHO}$  and  $\text{CH}_3\text{CO}$  has an activation barrier of  $53.0$  and  $59.4 \text{ kJ mol}^{-1}$ , respectively, which are favorable than  $\text{CH}_2\text{CO}$  hydrogenation to  $\text{CH}_2\text{COH}$  with the activation barrier of  $128.6 \text{ kJ mol}^{-1}$ . Meanwhile,  $\text{CH}_2\text{CO}$  has an adsorption energy of  $176.3 \text{ kJ mol}^{-1}$ , suggesting that  $\text{CH}_2\text{CO}$  prefers to be hydrogenated to  $\text{CH}_2\text{CHO}$  and  $\text{CH}_3\text{CO}$  rather than to be desorbed. Then, starting from  $\text{CH}_2\text{CHO}$  and  $\text{CH}_3\text{CO}$ , both can be hydrogenated to  $\text{CH}_3\text{CHO}$  with the corresponding activation barrier of  $42.9$  and  $57.1 \text{ kJ mol}^{-1}$ , respectively, which are much more favorable than  $\text{CH}_2\text{CHOH}$  and  $\text{CH}_3\text{COH}$  formation with the corresponding activation barriers of  $94.9$  and  $123.8 \text{ kJ mol}^{-1}$ . Moreover,  $\text{CH}_2\text{CHO}$  and  $\text{CH}_3\text{CO}$  have adsorption energies of  $279.8$  and  $257.4 \text{ kJ mol}^{-1}$ , respectively; therefore,  $\text{CH}_2\text{CHO}$  and  $\text{CH}_3\text{CO}$  prefer hydrogenation to  $\text{CH}_3\text{CHO}$  rather than their corresponding desorption. Similarly, starting from  $\text{CH}_3\text{CHO}$  with an adsorption energy of  $129.5 \text{ kJ mol}^{-1}$ ,  $\text{CH}_3\text{CHO}$  hydrogenation to  $\text{CH}_3\text{CH}_2\text{O}$  has the activation barrier of  $27.5 \text{ kJ mol}^{-1}$ , which is also more favorable than its desorption and  $\text{CH}_3\text{CHOH}$  formation. Further,  $\text{CH}_3\text{CH}_2\text{O}$  is hydrogenated to ethanol, which is endothermic by  $48.6 \text{ kJ mol}^{-1}$  with an activation barrier of  $109.6 \text{ kJ mol}^{-1}$ ;

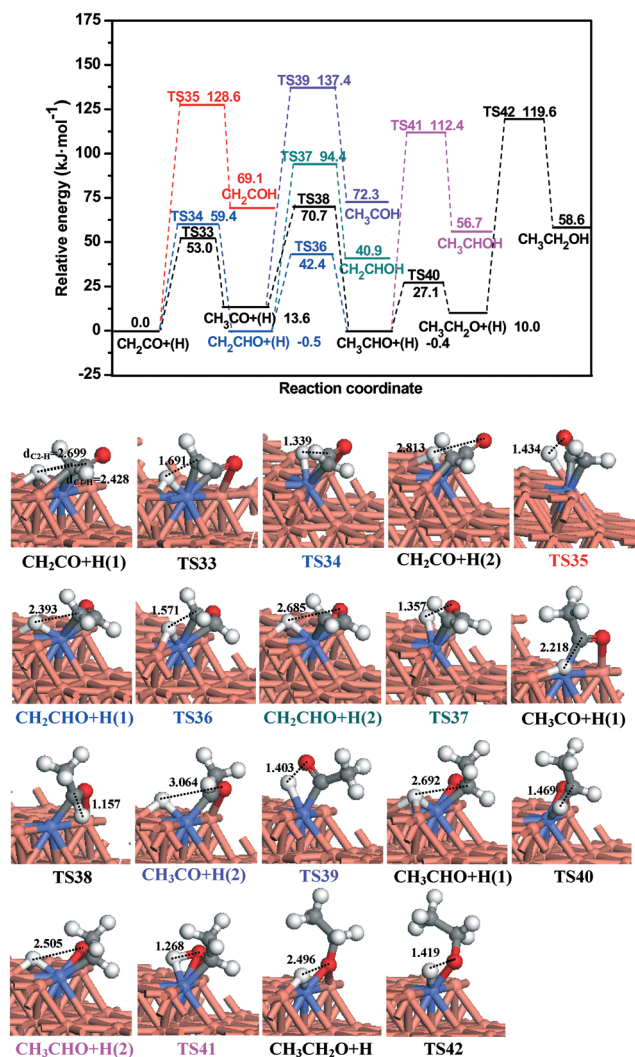


Fig. 10 The potential energy diagram of CH<sub>2</sub>CO hydrogenation to ethanol together with the structures of ISs and TSs. Bond lengths are in Å. See Fig. 2 for color coding.

CH<sub>3</sub>CH<sub>2</sub>O has an adsorption energy of 290.9 kJ mol<sup>-1</sup>, suggesting that CH<sub>3</sub>CH<sub>2</sub>O prefers hydrogenation to ethanol rather than its desorption.

### 3.6 Microkinetic modeling

In order to estimate the overall reaction rate ( $r$ ) and the rates for the major production of CH<sub>3</sub>OH ( $r_{\text{CH}_3\text{OH}}$ ), CH<sub>4</sub> ( $r_{\text{CH}_4}$ ), and C<sub>2</sub>H<sub>5</sub>OH ( $r_{\text{C}_2\text{H}_5\text{OH}}$ ) as well as their relative selectivity under typical experimental synthesis conditions ( $P_{\text{CO}} = 4$  atm,  $P_{\text{H}_2} = 8$  atm, and  $T = 500\text{--}600$  K), microkinetic modeling<sup>93–96</sup> has been employed on the CoCu(211) surface. For the microkinetic modeling in syngas conversion, the adsorption processes of CO and H<sub>2</sub> are assumed to be in equilibrium. Moreover, the pseudo-steady-state approximation<sup>93</sup> is applied to other minority species on the catalyst surface, namely, the production rates and the consumption rates of all species involved are thought to be the same. A detailed description of

the microkinetic model has been given in the ESI.† Table S1 lists all elementary steps involved in the optimal formation pathways of CH<sub>3</sub>OH, CH<sub>4</sub> and C<sub>2</sub>H<sub>5</sub>OH as well as the corresponding reaction rate constants at the temperature of 500, 525, 550, 575, and 600 K. The relative selectivity of the products CH<sub>4</sub>, CH<sub>3</sub>OH, and C<sub>2</sub>H<sub>5</sub>OH from syngas conversion on CoCu(211) at different temperatures is presented in Fig. 11. Here, the relative selectivity is defined by the relative rate for each product,  $r_i/(r_{\text{CH}_3\text{OH}} + r_{\text{CH}_4} + r_{\text{C}_2\text{H}_5\text{OH}})$ , where  $i$  is the species of the products.

On the CoCu(211) surface, the productivity of C<sub>2</sub>H<sub>5</sub>OH ( $r_{\text{C}_2\text{H}_5\text{OH}} = 1.40 \times 10^{-2}$  s<sup>-1</sup> per site) is higher than that of CH<sub>3</sub>OH ( $r_{\text{CH}_3\text{OH}} = 9.17 \times 10^{-4}$  s<sup>-1</sup> per site) and CH<sub>4</sub> ( $r_{\text{CH}_4} = 2.38 \times 10^{-3}$  s<sup>-1</sup> per site) at the temperature of 500 K; the same results can be also obtained under other temperatures. Previous studies<sup>96</sup> have proved that the interaction of CO with the surface plays an important role in the whole reaction, in which the weakening CO bonding can decrease the barrier for CO hydrogenation to CHO and increase the productivity. Therefore, in our studies, the weak adsorption energy of CO and the lower barrier for CO hydrogenation to CHO at the Cu site can accelerate the formation of CH<sub>3</sub>OH, CH<sub>4</sub> and C<sub>2</sub>H<sub>5</sub>OH. More importantly, generation of CH<sub>2</sub> and CH<sub>3</sub> species *via* H-assisted CH<sub>x</sub>O ( $x = 2, 3$ ) dissociation is more favorable than CH<sub>3</sub>OH formation. Thus, more CH<sub>2</sub> and CH<sub>3</sub> will be available for the formation of CH<sub>4</sub> and C<sub>2</sub> oxygenate C<sub>2</sub>H<sub>5</sub>OH.

As shown in Fig. 11, on the CoCu(211) surface, the relative selectivity of C<sub>2</sub>H<sub>5</sub>OH can reach approximately 80%, which is much higher than that of CH<sub>3</sub>OH and CH<sub>4</sub>; this result agrees well with the experimental results,<sup>27</sup> suggesting that the catalyst with the large Cu decorated by small Co nanoparticles improves alcohol selectivity, especially C<sub>2</sub>–C<sub>5</sub> alcohol, and decreases the selectivity of methanol as well as methane. With the increase in temperature from 500 to 600 K, the relative

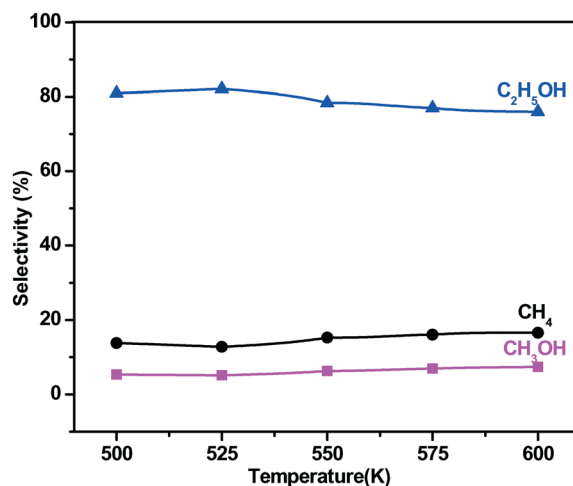


Fig. 11 The relative selectivity of products CH<sub>4</sub>, CH<sub>3</sub>OH, and C<sub>2</sub>H<sub>5</sub>OH from the syngas reaction on CoCu(211) at different temperatures using the microkinetic modeling technique.

selectivity of  $C_2H_5OH$  first rises and then moves down. Meanwhile, the variation trend of the relative selectivities of  $CH_3OH$  and  $CH_4$  is opposite to that of  $C_2H_5OH$ . Moreover, the relative selectivities of these products change slightly with the change in temperature. As a result, our designed Co-decorated Cu-based catalyst can improve the productivity and selectivity of ethanol significantly.

### 3.7 General discussion

Overall, the formation mechanism of  $C_2$  oxygenates from syngas has been systematically investigated using periodic DFT calculations on Co-decorated Cu(211) surfaces. The most favorable formation pathways of the possible products,  $C_2$  oxygenates  $C_2H_5OH$ ,  $CH_4$ , and  $CH_3OH$ , have been identified, in which ethanol is selected to model a high alcohol.

Fig. 12 presents the reaction mechanisms for the formation of  $C_2$  oxygenates and ethanol. Our results show that CO initial adsorption and activation occur at the Cu sites. CO prefers to be hydrogenated to CHO at the Cu site; subsequently, the CHO species at the Cu site easily migrates to the most stable Co–Cu mixed sites. Starting from CHO species adsorbed at Co–Cu mixed sites,  $CH_3OH$  is formed by the process  $CHO + H \rightarrow CH_2O + H \rightarrow CH_3O + H \rightarrow CH_3OH$ .  $CH_2$  and  $CH_3$  species are the most favorable  $CH_x$  monomers generated via H-assisted  $CH_xO$  ( $x = 2, 3$ ) dissociation, which is more fa-

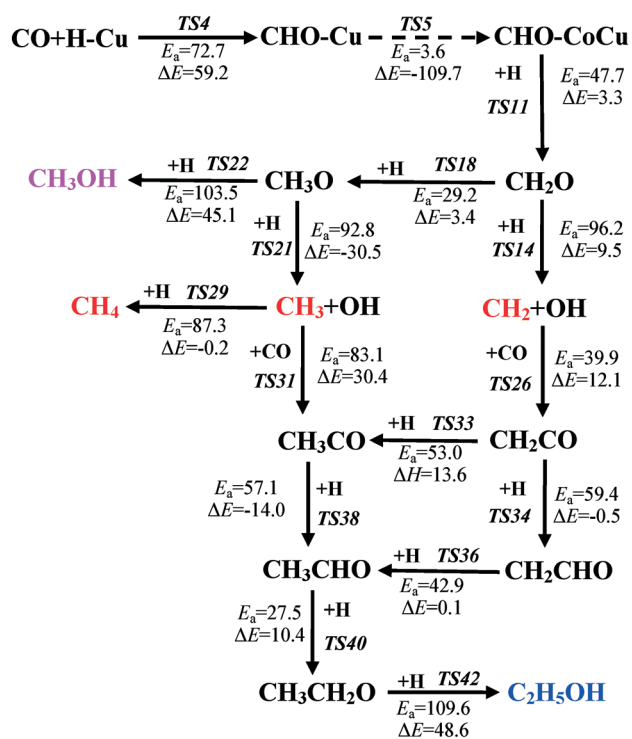
vorable than  $CH_3OH$  formation both thermodynamically and dynamically, suggesting that the CoCu(211) surface can provide more  $CH_x$  resources for the subsequent C–C chain formation in syngas conversion. Further, starting from  $CH_2$  and  $CH_3$  species,  $CH_4$  is generated by  $CH_2$  and  $CH_3$  hydrogenation; CO insertion into  $CH_2$  and  $CH_3$  species is the favorable pathway for the formation of  $C_2$  oxygenates  $CH_2CO$  and  $CH_3CO$ , which prefer to be successively hydrogenated to ethanol via  $CH_3CHO$  and  $CH_3CH_2O$  intermediates. Moreover, on the basis of microkinetic modeling, the selectivity of ethanol can reach approximately 80%, which is much higher than that of methanol and methane. As a result, ethanol is the predominant product in syngas conversion on the CoCu(211) surface.

**3.7.1 The active sites of the CoCu(211) surface.** On the basis of the above DFT calculations, in syngas conversion on the Co-decorated Cu(211) surface, except for the initial CO activation and hydrogenation to CHO species at the Cu site, it can be found that the adsorption of all species and all elementary reactions involved in syngas conversion occur at the Co sites or the Co–Cu mixed sites consisting of Co and Cu atoms rather than the Cu atoms, indicating that the surface Co sites or the Co–Cu mixed sites over Co-decorated Cu(211) are the active sites and exhibit the synergetic function between the active Co–Cu dual-sites for syngas conversion, which are in agreement with the previous experimental results.<sup>27,28</sup>

More importantly, CO hydrogenation to CHO at the Cu site is much more favorable than that at the Co–Cu mixed site both kinetically ( $72.7 \text{ kJ mol}^{-1}$  vs.  $112.7 \text{ kJ mol}^{-1}$ ) and thermodynamically ( $59.2 \text{ kJ mol}^{-1}$  vs.  $108.9 \text{ kJ mol}^{-1}$ ); subsequently, the facile diffusion of CHO species from the Cu site to the Co–Cu mixed site would increase the concentrations of CHO species at the Co–Cu mixed site, which also agrees with the previous studies.<sup>24</sup> Furthermore, starting from CHO adsorbed at the Co–Cu mixed site,  $CH_x$  ( $x = 2, 3$ ),  $CH_3OH$ ,  $CH_4$ , and  $C_2H_5OH$  are all generated at the Co–Cu mixed sites. Thus, the CHO intermediate plays an important role in syngas conversion over the CoCu(211) surface, and the CHO species at the Co–Cu mixed sites is predominantly responsible for the formation of  $CH_x$ ,  $CH_3OH$ ,  $CH_4$ , and ethanol.

In general, the Co sites or the Co–Cu mixed sites over the CoCu(211) surface are the active centers, which predominantly contribute to the formation of the key intermediates,  $CH_x$  ( $x = 2, 3$ ) and ethanol, and exhibit the synergetic function between the active Cu–Co dual sites for syngas conversion.

**3.7.2 Comparison of syngas conversion between Cu(211) and CoCu(211) surfaces.** For  $CH_x$  formation, our previous DFT studies on the pure Cu(211) surface<sup>20</sup> have suggested that  $CH_3$  is the most favorable monomer from syngas. However,  $CH_3OH$  formation is much more favorable kinetically than  $CH_3$  formation; thus, less surface concentration of  $CH_x$  monomers can be obtained to participate in the C–C chain formation, indicating that the Cu(211) surface exhibits good selectivity toward  $CH_3OH$  formation rather than hydrocarbons and ethanol, which accords with the general fact that



$E_a$  denotes the activation barrier for the corresponding step, and  $\Delta E$  represents the relevant reaction energy (unit:  $\text{kJ mol}^{-1}$ )

Fig. 12 Schematic of the optimal reaction pathway for  $C_2$  oxygenate and ethanol synthesis from syngas on the CoCu(211) surface.

Cu catalyst shows good catalytic performance for CH<sub>3</sub>OH formation from syngas. However, on the CoCu(211) surface, the most favorable CH<sub>x</sub> monomers are CH<sub>2</sub> and CH<sub>3</sub> species. Moreover, the formation of CH<sub>2</sub> and CH<sub>3</sub> species is more favorable than CH<sub>3</sub>OH formation both thermodynamically and dynamically, suggesting that compared to the pure Cu(211) surface, the Co-decorated Cu(211) surface exhibits a good selectivity toward the formation of CH<sub>2</sub> and CH<sub>3</sub> species rather than CH<sub>3</sub>OH in syngas conversion.

On the other hand, for C<sub>2</sub> oxygenate formation over the CoCu(211) surface, CH<sub>2</sub>CO and CH<sub>3</sub>CO are the major C<sub>2</sub> oxygenates generated from CO insertion into CH<sub>2</sub> and CH<sub>3</sub> species, respectively. CH<sub>2</sub>CO prefers to be hydrogenated to CH<sub>2</sub>-CHO and CH<sub>3</sub>CO, followed by the successive hydrogenation to ethanol *via* CH<sub>3</sub>CHO and CH<sub>3</sub>CH<sub>2</sub>O intermediates; ethanol is selected to model a high alcohol. Moreover, based on microkinetic modeling, the selectivity of C<sub>2</sub>H<sub>5</sub>OH can reach approximately 80%, which is much higher than that of CH<sub>3</sub>-OH and CH<sub>4</sub>. These results show that ethanol is the predominant product in syngas conversion on the CoCu(211) surface. On Cu(211) surface,<sup>20</sup> once the most favorable monomer CH<sub>3</sub> is formed, CO insertion into CH<sub>3</sub> to CH<sub>3</sub>CO formation is the most favorable; subsequently, CH<sub>3</sub>CO is successively hydrogenated to ethanol *via* CH<sub>3</sub>COH and CH<sub>3</sub>CHOH intermediates. However, CH<sub>3</sub>OH formation is more favorable than CH<sub>3</sub> formation; as a result, fewer CH<sub>3</sub> sources can be obtained to participate in C–C chain formation, and the productivity and selectivity of ethanol from syngas is very low due to fewer CH<sub>3</sub> sources and more CH<sub>3</sub>OH formation.

Therefore, compared to the pure Cu(211) surface, the CoCu(211) surface with Co-promoted Cu catalyst not only promotes the formation of CH<sub>x</sub> species and ethanol but also suppresses CH<sub>3</sub>OH formation. As a result, the productivity and selectivity of ethanol can be significantly improved, namely, the CoCu(211) surface exhibits a relatively good selectivity toward ethanol as a model high alcohol rather than the dominant product CH<sub>3</sub>OH on Cu(211) surface.

**3.7.3 The role of Cu and Co.** Clearly, upon alloying with Co, the selectivity to ethanol is significantly improved over Co-decorated Cu catalysts. Thus, we further identify the role of Cu and Co according to the comparisons between CoCu(211) and Cu(211) surfaces.<sup>20</sup>

It is well-known that Cu alone is inactive in breaking the C–O bond, which favors CO hydrogenation to CHO<sup>20,97–99</sup> over Co-decorated Cu(211) surface. The adsorption and activation of CO to form CHO firstly occur at the Cu site, and subsequently CHO easily migrates from the Cu site to the most stable Co–Cu mixed site. Compared to CHO adsorption at the Cu sites, the enhanced adsorption ability of CHO at Co–Cu mixed sites becomes a thermodynamic driving force to lower the barrier for CHO diffusion from the Cu site to Co–Cu mixed sites (155.1 *vs.* 252.9 kJ mol<sup>-1</sup>). The stronger interaction between the catalyst and the adsorbed CHO species is attributed to more electron transfers between the surface Cu/Co atoms and CHO species. The Bader charge of CHO adsorbed at the Co–Cu mixed site is 0.35 e, while it is

decreased to 0.30 e at the Cu site; meanwhile, the projected density of state (pDOS) of CHO adsorbed at the Cu site and Co–Cu mixed sites on the CoCu(211) surface (see Fig. 13) shows that the overlap between the p-orbital of C and O atoms and the d-orbital of Cu and Co atoms is increased when CHO is adsorbed from the Cu site to the Co–Cu mixed sites; thus, the interaction between the CHO site and the Co–Cu mixed site is enhanced. On the other hand, direct dissociation of CO at the Co site or the Co–Cu dual-site is suppressed due to the high barrier of 387.4 kJ mol<sup>-1</sup>, which reduces the surface concentration of coupling monomers, CH<sub>x</sub> species, in the initial CO activation stage and therefore suppresses CH<sub>x</sub> coupling reactions. Compared to the Co-based catalysts, this may be one of the reasons why the Co-decorated Cu-based catalyst shows poor selectivity to C<sub>2</sub> hydrocarbons.

The Cu species provides the active sites for CO adsorption and CO hydrogenation to CHO. The Co species is slightly negatively charged than the Cu species,<sup>100</sup> and electron transfer from surface Cu to Co species occurs, which is proved by experimental XPS data.<sup>27</sup> Our differential charge density of the Co atom and its surrounding surface Cu atoms over a CoCu(211) surface and Cu atoms over a Cu(211) surface (see Fig. 14) shows that there is more charge transfer between the Co atom and its surrounding surface Cu atoms over the CoCu(211) surface than that between Cu atoms over the Cu(211) surface, suggesting that Cu makes its electrons available to the Co atom over the CoCu(211) surface, namely, the electron transferred from the surface Cu to Co. Moreover, Bader charge analysis on CoCu(211) shows that the electron transferred from the surface Cu to Co is only 0.01 e, namely, the electron transferred from the surface Cu to Co is negligible, which is consistent with the previous experimental

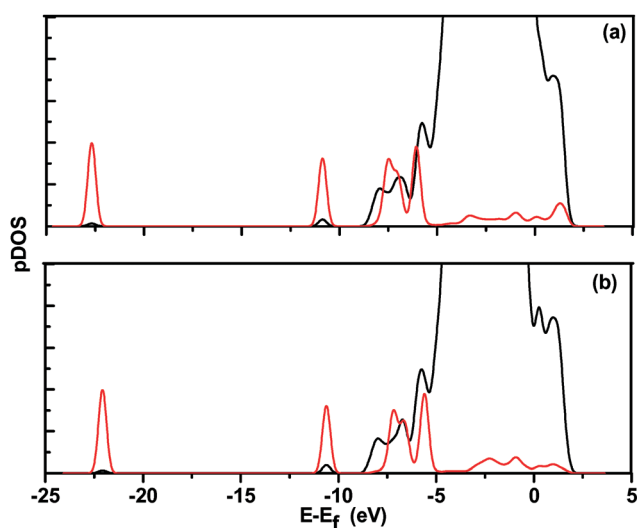


Fig. 13 Projected density of state (pDOS) of CHO adsorbed at the (a) Cu site and (b) Co–Cu mixed sites on CoCu(211) surface. The p orbital of C and O atoms (red line) and the d orbital of Cu and Co atoms (black line).

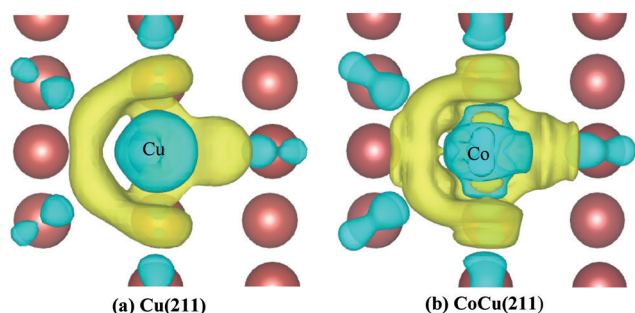


Fig. 14 The differential charge density of (a) Cu atoms over Cu(211) surface and (b) Co atom and its surrounding Cu atoms over CoCu(211) surface. The blue and yellow shaded regions represent charge loss and charge gain, respectively.

studies.<sup>27,100</sup> The decreasing electron density of Cu facilitates the formation of CHO species by CO hydrogenation compared to that of the pure Cu(211) surface. On the other hand, CHO easily diffuses to the Co–Cu mixed sites, which increases the surface concentration of CHO species. Thus, Cu mainly serves as the reservoir for the key intermediates CO/CHO, which is consistent with the “dual-site” mechanism.<sup>101,102</sup>

However, Co alone is active in breaking the C–O bond,<sup>103–105</sup> which is the prerequisite for initiating CH<sub>x</sub> formation and C–C chain formation. Our results show that all species prefer to interact with Co atoms or the sites consisting of Co and Cu atoms rather than the Cu atoms, namely, the enhanced adsorption of small species, especially for CH<sub>x</sub> ( $x = 1–3$ ), C, O, OH, and CH<sub>x</sub>O at the Co site or the Co–Cu dual-site becomes a thermodynamic driving force to lower the barrier for the C–O bond breaking reaction. As mentioned above, with the addition of Co, the CH<sub>x</sub>–O ( $x = 1–3$ ) bond cleavage steps are all promoted, indicating that Co species can facilitate the formation of CH<sub>x</sub> ( $x = 2, 3$ ) species and increase the concentration of CH<sub>x</sub> ( $x = 2, 3$ ) species adsorbed at the Co–Cu mixed sites. More importantly, due to the easier CH<sub>x</sub>–O ( $x = 1–3$ ) bond cleavage step, the Co species suppresses the formation of CH<sub>3</sub>OH and improves the selectivity of the monomers, CH<sub>2</sub> and CH<sub>3</sub> species; meanwhile, the Co–Cu dual-sites facilitate CO insertion into CH<sub>2</sub> and CH<sub>3</sub> species.

As mentioned above, Cu provides the undissociated CO/CHO, whereas Co promotes CH<sub>x</sub> formation and facilitates the C–C chain formation. The synergetic effect between the active Co and Cu sites improves the productivity and selectivity of ethanol significantly. Either an electronic effect or a geometric effect has been proposed to explain how the synergetic interaction between two components affects the catalytic behaviors of bimetallic catalysts. The Bader charge analysis indicated above shows that only a negligible charge transfer (0.01 e) occurs between Co and Cu. Thus, the addition of Cu takes effect on the geometry of ensembles rather than electronic property. Recently, a comparative experimental study of higher alcohol synthesis from syngas over monome-

tallic Co and bimetallic Cu-decorated Co/SiO<sub>2</sub> catalysts has been performed to probe into the role of Cu using *ex situ* XRD, XAS and Raman spectroscopy,<sup>106</sup> suggesting that the role of Cu is to weaken CO/HCO dissociation, reduce the formation of CH<sub>x</sub> species, and inhibit C–C chain formation; this experimental study further confirms the roles of Co and Cu over Co-decorated Cu-based catalyst in this study.

## 4. Conclusions

Periodic DFT and microkinetic modeling calculations have been performed to investigate the formation mechanism of C<sub>2</sub> oxygenates and ethanol from syngas over a Co-decorated Cu-based catalyst (CoCu(211) surface), and the results are expected to probe into the roles of Co and Cu as well as identify the catalytic selectivity toward C<sub>2</sub> species based on the less expensive Cu-based catalyst. The following results are obtained:

On the CoCu(211) surface, our results show that CO initial adsorption and activation occur at the Cu sites and CO prefers to be hydrogenated to CHO at the Cu site, and subsequently, CHO species at the Cu site easily migrate to the most stable Co–Cu mixed sites. Starting from CHO species adsorbed at Co–Cu mixed sites, CH<sub>2</sub> and CH<sub>3</sub> species are the most favorable CH<sub>x</sub> monomers generated *via* H-assisted CH<sub>x</sub>–O ( $x = 2, 3$ ) dissociation, which is more favorable than CH<sub>3</sub>–OH formation both thermodynamically and dynamically, whereas on the pure Cu(211) surface, CH<sub>3</sub> is the most favorable monomer; however, CH<sub>3</sub>OH formation is much more favorable kinetically than CH<sub>3</sub> formation. Meanwhile, starting from CH<sub>2</sub> and CH<sub>3</sub> species, the C<sub>2</sub> oxygenates CH<sub>2</sub>CO and CH<sub>3</sub>CO are the major products from syngas other than C<sub>2</sub> hydrocarbons or CH<sub>4</sub>. Further, CH<sub>2</sub>CO and CH<sub>3</sub>CO prefer to be successively hydrogenated to ethanol *via* CH<sub>2</sub>CHO, CH<sub>3</sub>CHO, and CH<sub>3</sub>CH<sub>2</sub>O intermediates. Moreover, on the basis of microkinetic modeling, the CoCu(211) surface shows high selectivity for ethanol rather than methanol and methane; namely, compared to the Cu(211) surface, the CoCu(211) surface significantly improves the productivity and selectivity of ethanol.

On the other hand, the roles of Co and Cu have been identified. The function of Cu is to provide the undissociated CO/CHO at the Cu sites, whereas Co promotes CH<sub>x</sub> formation by accelerating C–O bond cleavage and facilitating C–C chain formation, which is the so-called dual-site mechanism. The synergetic effect between the active Co and Cu sites is predominantly responsible for the formation of C<sub>2</sub> oxygenates and ethanol. Meanwhile, we believe that the insight derived from this study can provide a basis for the catalyst design of C<sub>2</sub> oxygenate synthesis from syngas over the less expensive Cu-based catalysts.

## Acknowledgements

This work is financially supported by the National Natural Science Foundation of China (No. 21276003, 21476155 and

21276171), the Natural Science Foundation of Shanxi Province (No. 2014011012-2), the Program for the Top Young Academic Leaders of Higher Learning Institutions of Shanxi, and the Top Young Innovative Talents of Shanxi.

## References

- 1 S. Velu, N. Satoh, C. S. Gopinath and K. Suzuki, *Catal. Lett.*, 2002, **82**, 145–152.
- 2 D. A. Deluga, J. R. Salge, L. D. Schmidt and X. E. Verykios, *Science*, 2004, **303**, 993–997.
- 3 C. S. Song, *Catal. Today*, 2006, **115**, 2–32.
- 4 J. J. Spivey and A. Egbibi, *Chem. Soc. Rev.*, 2007, **36**, 1514–1528.
- 5 M. Gupta, M. L. Smith and J. J. Spivey, *ACS Catal.*, 2011, **1**, 641–656.
- 6 V. Subramani and S. K. Gangwal, *Energy Fuels*, 2008, **22**, 814–839.
- 7 P. Forzatti, E. Tronconi and I. Pasquon, *Catal. Rev.: Sci. Eng.*, 1991, **33**, 109–168.
- 8 K. G. Fang, D. B. Li, M. G. Lin, M. L. Xiang, W. Wei and Y. H. Sun, *Catal. Today*, 2009, **147**, 133–138.
- 9 Y. Z. Fang, Y. Liu and L. H. Zhang, *Appl. Catal., A*, 2011, **397**, 183–191.
- 10 A. Cosultchi, M. Perez-Luna, J. A. Morales-Serna and M. Salmon, *Catal. Lett.*, 2012, **142**, 368–377.
- 11 J. J. Wang, P. A. Chernavskii, Y. Wang and A. Y. Khodakov, *Fuel*, 2013, **103**, 1111–1122.
- 12 G. L. Liu, Y. X. Geng, D. M. Pan, Y. Zhang, T. Niu and Y. Liu, *Fuel Process. Technol.*, 2014, **128**, 289–296.
- 13 G. L. Liu, D. M. Pan, T. Niu, A. Cao, Y. Z. Yue and Y. Liu, *RSC Adv.*, 2015, **5**, 31637–31647.
- 14 Y. Z. Xiang, R. Barbosa, X. N. Li and N. Kruse, *ACS Catal.*, 2015, **5**, 2929–2934.
- 15 M. G. Lin, K. G. Fang, D. B. Li and Y. H. Sun, *Catal. Commun.*, 2008, **9**, 1869–1873.
- 16 M. Y. Ding, J. L. Tu, J. G. Liu, N. Tsubaki, T. J. Wang and L. L. Ma, *Catal. Today*, 2014, **234**, 278–284.
- 17 Y. W. Liu, F. Yu, J. Hu and J. Liu, *Appl. Catal., A*, 2012, **429–430**, 48–58.
- 18 A. Kiennemann, A. Barama, S. Boujana and M. M. Bettahar, *Appl. Catal., A*, 1993, **99**, 175–194.
- 19 Y. H. Zhao, M. M. Yang, D. P. Sun, H. Y. Su, K. J. Sun, X. F. Ma, X. H. Bao and W. X. Li, *J. Phys. Chem. C*, 2011, **115**, 18247–18256.
- 20 R. G. Zhang, G. R. Wang and B. J. Wang, *J. Catal.*, 2013, **305**, 238–255.
- 21 Y. Z. Xiang, V. Chitry, P. Liddicoat, P. Felfer, J. Cairney, S. Ringer and N. Kruse, *J. Am. Chem. Soc.*, 2013, **135**, 7114–7117.
- 22 G. Prieto, S. Beijer, M. L. Smith, M. He, Y. Au, Z. Wang, D. A. Bruce, K. P. de Jong, J. J. Spivey and P. E. de Jongh, *Angew. Chem., Int. Ed.*, 2014, **53**, 6397–6401.
- 23 X. H. Mo, Y. T. Tsai, J. Gao, D. S. Mao and J. G. Goodwin Jr, *J. Catal.*, 2012, **285**, 208–215.
- 24 X. C. Xu, J. J. Su, P. F. Tian, D. L. Fu, W. W. Dai, W. Mao, W. K. Yuan, J. Xu and Y. F. Han, *J. Phys. Chem. C*, 2015, **119**, 216–227.
- 25 N. D. Subramanian, G. Balaji, C. S. S. R. Kumar and J. J. Spivey, *Catal. Today*, 2009, **147**, 100–106.
- 26 J. Anton, J. Nebel, H. Q. Song, C. Froese, P. Weide, H. Ruland, M. Muhler and S. Kaluza, *Appl. Catal., A*, 2015, **505**, 326–333.
- 27 Y. P. Pei, S. P. Jian, Y. Y. Chen and C. C. Wang, *RSC Adv.*, 2015, **5**, 76330–76336.
- 28 W. Gao, Y. F. Zhao, H. R. Chen, H. Chen, Y. Li, W. S. He, Y. K. Zhang, M. Wei, D. G. Evans and X. Duan, *Green Chem.*, 2015, **17**, 1525–1534.
- 29 Y. H. Zhao, K. J. Sun, X. F. Ma, J. X. Liu, D. P. Sun, H. Y. Su and W. X. Li, *Angew. Chem., Int. Ed.*, 2011, **50**, 5335–5338.
- 30 L. P. Han, D. S. Mao, J. Yu, Q. S. Guo and G. Z. Lu, *Catal. Commun.*, 2012, **23**, 20–24.
- 31 J. Cheng, P. Hua, P. Ellis, S. French, G. Kelly and C. Martin Lok, *J. Catal.*, 2008, **257**, 221–228.
- 32 G. G. Volkova, T. M. Yurieva, L. M. Plyasova, M. I. Naumova and V. I. Zaikovskii, *J. Mol. Catal. A: Chem.*, 2000, **158**, 389–393.
- 33 K. Xiao, X. Z. Qi, Z. H. Bao, X. X. Wang, L. S. Zhong, K. G. Fang, M. G. Lin and Y. H. Sun, *Catal. Sci. Technol.*, 2013, **3**, 1591–1602.
- 34 S. Y. Deng, W. Chu, H. Y. Xu, L. M. Shi and L. H. Huang, *J. Nat. Gas Chem.*, 2008, **17**, 369–373.
- 35 K. Xiao, Z. H. Bao, X. Z. Qi, X. X. Wang, L. S. Zhong, K. G. Fang, M. G. Lin and Y. H. Sun, *Chin. J. Catal.*, 2013, **34**, 116–129.
- 36 J. B. Wang, X. R. Zhang, Q. Sun, S. Chan and H. B. Su, *Catal. Commun.*, 2015, **61**, 57–61.
- 37 X. Dong, X. L. Liang, H. Y. Li, G. D. Lin, P. Zhang and H. B. Zhang, *Catal. Today*, 2009, **147**, 158–165.
- 38 J. Wang, P. A. Chernavskii, A. Y. Khodakov and Y. Wang, *J. Catal.*, 2012, **286**, 51–61.
- 39 A. Cao, G. L. Liu, Y. Z. Yue, L. H. Zhang and Y. Liu, *RSC Adv.*, 2015, **5**, 58804–58812.
- 40 J. Anton, J. Nebel, H. Q. Song, C. Froese, P. Weide, H. Ruland, M. Muhler and S. Kaluza, *J. Catal.*, 2016, **33**, 175–186.
- 41 A. L. Rocha, I. G. Solórzano and J. B. Vander Sande, *Mater. Sci. Eng., C*, 2007, **27**, 1215–1221.
- 42 J. J. Wang, P. A. Chernavskii, A. Y. Khodakov and Y. Wang, *J. Catal.*, 2012, **286**, 51–61.
- 43 A. S. Edelstein, V. G. Harris, D. R. Rolinson and L. Kurihara, *Appl. Phys. Lett.*, 1999, **74**, 3161–3163.
- 44 S. Carencu, A. Tuxen, M. Chintapalli, E. Pach, C. Escudero, T. D. Ewers, P. Jiang, F. Borondics, G. Thornton, A. P. Alivisatos, H. Bluhm, J. H. Guo and M. Salmeron, *J. Phys. Chem. C*, 2013, **117**, 6259–6266.
- 45 S. X. Yin, X. Y. Ma and D. E. Ellis, *Surf. Sci.*, 2007, **601**, 2426–2437.
- 46 J. A. Rodriguez, J. C. Hanson, A. I. Frenkel, J. Y. Kim and M. Pérez, *J. Am. Chem. Soc.*, 2002, **124**, 346–354.
- 47 R. G. Zhang, B. J. Wang, L. X. Ling, H. Y. Liu and W. Huang, *Appl. Surf. Sci.*, 2010, **257**, 1175–1180.

- 48 R. G. Zhang, H. Y. Liu, H. Y. Zheng, L. X. Ling, Z. Li and B. J. Wang, *Appl. Surf. Sci.*, 2011, **257**, 4787–4794.
- 49 R. G. Zhang, H. Y. Liu, J. R. Li, L. X. Ling, Z. Li and B. J. Wang, *Appl. Surf. Sci.*, 2012, **258**, 9932–9943.
- 50 Y. Xu and M. Mavrikakis, *J. Phys. Chem. B*, 2003, **107**, 9298–9307.
- 51 M. Mavrikakis, M. Bäumer, H. J. Freund and J. K. Nørskov, *Catal. Lett.*, 2002, **81**, 153–156.
- 52 L. Olsson, V. P. Zhdanov and B. Kasemo, *Surf. Sci.*, 2003, **529**, 338–348.
- 53 F. A. Pedersen, J. Greeley and J. K. Nørskov, *Catal. Lett.*, 2005, **105**, 9–13.
- 54 B. McAllister and P. Hu, *J. Chem. Phys.*, 2005, **122**, 084709.
- 55 Z. P. Liu and P. Hu, *J. Am. Chem. Soc.*, 2003, **125**, 1958–1967.
- 56 B. Hammer, *J. Catal.*, 2001, **199**, 171–176.
- 57 J. Zhang, X. M. Cao, P. Hu, Z. Y. Zhong, A. Borgna and P. Wu, *J. Phys. Chem. C*, 2011, **115**, 22429–22437.
- 58 T. Zamvelli, J. Wintterlin, J. Throst and G. Ertl, *Science*, 1996, **273**, 1688–1690.
- 59 R. C. Catapan, A. A. M. Oliveira, Y. Chen and D. G. Vlachos, *J. Phys. Chem. C*, 2012, **116**, 20281–20291.
- 60 M. Behrens, F. Studt, I. Kasatkin, S. Kühn, M. Hävecker, F. Abild-Pedersen, S. Zander, F. Girgsdies, P. Kurr, B. L. Kniep, M. Tovar, R. W. Fischer, J. K. Nørskov and R. Schlögl, *Science*, 2012, **336**, 893–897.
- 61 N. Kapur, J. Hyun, B. Shan, J. B. Nicholas and K. Cho, *J. Phys. Chem. C*, 2010, **114**, 10171–10182.
- 62 S. González, D. Loffreda, P. Sautet and F. Illas, *J. Phys. Chem. C*, 2007, **111**, 11376–11383.
- 63 K. Sumida, D. Stuck, L. Mino, J. D. Chai, E. D. Bloch, O. Zavorotynska, L. J. Murray, M. Dinca, S. Chavan, S. Bordiga, M. Head-Gordon and J. R. Long, *J. Am. Chem. Soc.*, 2013, **135**, 1083–1091.
- 64 H. H. Kim, J. W. Yang, S. B. Jo, B. Kang, S. K. Lee, H. Bong, G. Lee, K. S. Kim and K. Cho, *ACS Nano*, 2013, **7**, 1155–1162.
- 65 G. Kresse and J. Furthmuller, *Phys. Rev. B: Condens. Matter Mater. Phys.*, 1996, **54**, 11169–11186.
- 66 G. Kresse and J. Furthmuller, *Comput. Mater. Sci.*, 1996, **6**, 15–50.
- 67 P. E. Blöchl, *Phys. Rev. B: Condens. Matter Mater. Phys.*, 1994, **50**, 17953–17979.
- 68 G. Kresse and D. Joubert, *Phys. Rev. B: Condens. Matter Mater. Phys.*, 1999, **59**, 1758–1775.
- 69 J. P. Perdew, K. Burke and M. Ernzerhof, *Phys. Rev. Lett.*, 1996, **77**, 3865–3868.
- 70 J. P. Perdew and Y. Wang, *Phys. Rev. B: Condens. Matter Mater. Phys.*, 1992, **45**, 13244–13249.
- 71 S. G. Louie, S. Froyen and M. L. Cohen, *Phys. Rev. B: Condens. Matter Mater. Phys.*, 1982, **26**, 1738–1742.
- 72 Q. Ge, M. Neurock, H. A. Wright and N. Srinivasan, *J. Phys. Chem. B*, 2002, **106**, 2826–2829.
- 73 L. Joos, I. A. W. Filot, S. Cottenier, E. J. M. Hensen, M. Waroquier, V. V. Speybroeck and R. A. van Santen, *J. Phys. Chem. C*, 2014, **118**, 5317–5327.
- 74 D. Sheppard, P. Xiao, W. Chemelewski, D. D. Johnson and G. Henkelman, *J. Chem. Phys.*, 2012, **136**, 074103.
- 75 D. Sheppard, R. Terrell and G. Henkelman, *J. Chem. Phys.*, 2008, **128**, 134106.
- 76 G. Henkelman and H. Jónsson, *J. Chem. Phys.*, 1999, **111**, 7010–7022.
- 77 R. A. Olsen, G. J. Kroes, G. Henkelman, A. Arnaldsson and H. Jónsson, *J. Chem. Phys.*, 2004, **121**, 9776–9792.
- 78 N. Kapur, J. Hyun, B. Shan, J. B. Nicholas and K. Cho, *J. Phys. Chem. C*, 2010, **114**, 10171–10182.
- 79 J. P. Clay, J. P. Greeley, F. H. Ribeiro, W. N. Delgass and W. F. Schneider, *J. Catal.*, 2014, **320**, 106–117.
- 80 C. M. Truong, J. A. Rodriguez and D. W. Goodman, *Surf. Sci.*, 1992, **271**, L385–L391.
- 81 G. A. Beitel, C. P. M. de Groot, H. Oosterbeek and J. H. Wilson, *J. Phys. Chem. B*, 1997, **101**, 4035–4043.
- 82 O. R. Inderwildi, S. J. Jenkins and D. A. King, *J. Phys. Chem. C*, 2008, **112**, 1305–1307.
- 83 P. V. Helden, J. A. V. D. Berg and I. M. Ciobică, *Catal. Sci. Technol.*, 2012, **2**, 491–494.
- 84 C. Chen, Q. Wang, G. Wang, B. Hou, L. Jia and D. Li, *J. Phys. Chem. C*, 2016, **120**, 9132–9147.
- 85 A. Deluzarche, J. P. Hindermann, R. Kieffer, R. Breault and A. Kiennemann, *J. Phys. Chem.*, 1984, **88**, 4993–4995.
- 86 A. Kiennemann, R. Breault, J. P. Hindermann and M. Laurin, *J. Chem. Soc., Faraday Trans. 1*, 1987, **83**, 2119–2128.
- 87 C. Diagne, H. Idriss, J. P. Hindermann and A. Kiennemann, *Appl. Catal.*, 1989, **51**, 165–180.
- 88 I. N. Remediakis, F. Abild-Pedersen and J. K. Nørskov, *J. Phys. Chem. B*, 2004, **108**, 14535–14540.
- 89 R. G. Zhang, F. Liu, X. J. Zhao, B. J. Wang and L. X. Ling, *J. Phys. Chem. C*, 2015, **119**, 10355–10364.
- 90 M. K. Zhuo, A. Borgn and M. Saeys, *J. Catal.*, 2013, **297**, 217–226.
- 91 M. Ojeda, R. Nabar, A. U. Nilekar, A. Ishikawa, M. Mavrikakis and E. Iglesia, *J. Catal.*, 2010, **272**, 287–297.
- 92 J. B. Wang, Q. Sun, S. Chan and H. B. Su, *Appl. Catal., A*, 2016, **509**, 97–104.
- 93 P. Liu, A. Logadottir and J. K. Nørskov, *Electrochim. Acta*, 2003, **48**, 3731–3742.
- 94 P. Liu and J. A. Rodriguez, *J. Chem. Phys.*, 2007, **126**, 164705.
- 95 P. Liu and J. A. Rodriguez, *J. Phys. Chem. B*, 2006, **110**, 19418–19425.
- 96 Y. M. Choi and P. Liu, *J. Am. Chem. Soc.*, 2009, **36**, 13054–13061.
- 97 X. C. Sun, R. G. Zhang and B. J. Wang, *Appl. Surf. Sci.*, 2013, **265**, 720–730.
- 98 R. G. Zhang, X. C. Sun and B. J. Wang, *J. Phys. Chem. C*, 2013, **117**, 6594–6606.
- 99 H. Y. Zheng, R. G. Zhang, Z. Li and B. J. Wang, *J. Mol. Catal. A: Chem.*, 2015, **404**, 115–130.
- 100 A. Y. Yin, C. Wen, X. Y. Guo, W. L. Dai and K. N. Fan, *J. Catal.*, 2011, **280**, 77–88.

- 101 R. M. Bailliard-Letournel, A. J. Gomez Cobo, C. Mirodatos, M. Primet and J. A. Dalmon, *Catal. Lett.*, 1989, 2, 149–156.
- 102 J. A. Dalmon, P. Chaumette and C. Mirodatos, *Catal. Today*, 1992, 15, 101–127.
- 103 C. F. Huo, Y. W. Li, J. G. Wang and H. J. Jiao, *J. Phys. Chem. C*, 2008, 112, 14108–14116.
- 104 J. X. Liu, H. Y. Su, D. P. Sun, B. Y. Zhang and W. X. Li, *J. Am. Chem. Soc.*, 2013, 135, 16284–16287.
- 105 Y. H. Zhao, J. X. Liu, H. Y. Su, K. J. Sun and W. X. Li, *ChemCatChem*, 2014, 6, 1755–1762.
- 106 J. J. Su, Z. P. Zhang, D. L. Fu, D. Liu, X. C. Xu, B. F. Shi, X. Wang, R. Si, Z. Jiang, J. Xu and Y. F. Han, *J. Catal.*, 2016, 336, 94–106.